Results in Engineering 30 (2026) 110675

Contents lists available at ScienceDirect

Results in Engineering

journal homepage: www.sciencedirect.com/journal/results-in-engineering

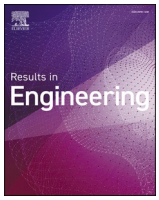

Research paper

Tensile and flexural performance of FDM 3D printed Harakeke (NZ Flax) fiber -PLA composites for lightweight structural applications

S.K. Selvamani [a], K.S. Clint [a], M. Samykano [b,*], K. Kadirgama [a], M.D.H. Beg [c], K.L. Pickering [c], A. Megalingam [a]

[a] Faculty of Mechanical and Automotive Engineering Technology, University Malaysia Pahang Al-Sultan Abdullah (UMPSA), 26600 Pekan, Pahang, Malaysia
[b] Mechanical and Aerospace Engineering Department, College of Engineering, United Arab Emirates University, Al Ain 15551, United Arab Emirates
[c] School of Engineering, University of Waikato, Private Bag 3105, Hamilton, New Zealand

ARTICLE INFO

Keywords:
3D printing
New Zealand flax
PLA composites
Tensile properties
Flexural properties
Response surface methodology

ABSTRACT

Current research on the shift toward sustainable materials has intensified interest in biodegradable alternatives polymers, with poly-lactic acid (PLA) emerging as a leading candidate. With various advantages, including biodegradability and processability, PLA's tensile and flexural strength can be further enhanced to increase its use in lightweight structural applications. This study introduces a novel integration of harakeke (New Zealand flax) fibers into PLA, a material pairing that has not been comprehensively investigated for additive manufacturing-based components. The research uniquely employs a Response Surface Methodology (RSM)-based optimization framework to systematically analyze and model the combined effects of fiber content (0-20 wt.%), raster angle (45-90°), and raster width (0.5-1.0 mm) on the composite's tensile and flexural performance. The findings reveal that a raster width of 0.5 mm, raster angle of 45°, and a flax infill of 10% by weight provide the best synergy of stiffness and strength. The maximum values of Young's modulus are 4453.85 MPa, and the flexural stress is 73.395 MPa. Increased fiber loadings above 20 wt.% reduce performance due to fiber agglomeration. Among orientations, the 45° raster is preferable to 90° due to increased load transfer and stress distribution, and narrower raster widths facilitate greater interlayer bonding and deposition density.

1. Introduction

In recent years, efforts have been increasing to develop sustainable alternatives to petroleum-derived polymers through the integration of green chemistry, sustainability, and environmental efficiency principles. Poly lactic acid (PLA), which is a highly processable and biodegradable polymer, presents an extensive and environmentally efficient substitute for traditional non-degradable plastics with adequate strength and stiffness for varied packaging, biomedical, and lightweight applications where environmental sustainability is more important than excessive load-bearing requirements [1,2]. However, previous research results reveal that its inherent brittleness [3,4] and limited mechanical strength limits its use in structural or load-bearing applications. The addition of natural fiber reinforcements has been shown to be an efficient and sustainable method to improve the mechanical performance of PLA, Natural fibers like sisal, hemp, flax, jute, and oil palm are desirable due to their high strength-to-weight ratio, biodegradability, and lack of abrasiveness [5,6]. Fiber loading and treatment have major effects on interfacial adhesion and composite performance, and untreated fibers generally create weak interfaces at the expense of mechanical integrity [7]. Researchers suggest that harakeke (New Zealand flax), composed of sclerenchyma fibers embedded in lignin and hemicellulose, is a sustainable and culturally important reinforcement. Additive manufacturing, as exemplified by fused deposition modelling (FDM), has potential for tailor-made lightweight composites but poses issues not present in traditional processing. Mechanical performance is strongly affected by layer adhesion, void formation, fiber dispersion, and thermal degradation. Raster angle, raster width, and layer height are important FDM parameters that control load transfer and anisotropy in printed components, but most research on natural fiber-reinforced PLA ignores these effects, leading to unreproducible results and poor scalability [8,9].

A statistically driven optimization framework is accurate and easy to systematically evaluate how multiple FDM parameters and fiber interactions affect joint behavior, which in turn enables accurate modeling and prediction of mechanical responses [10]. Previous related research

* Corresponding author.
E-mail address: mahendran@uaeu.ac.ae (M. Samykano).

https://doi.org/10.1016/j.rineng.2026.110675
Received 13 February 2026; Received in revised form 11 April 2026; Accepted 22 April 2026
Available online 24 April 2026

results suggest that instead of using trial and error approaches, statistical methods such as RSM or ANOVA can be used with Design Expert or Minitab software. The rationale for adopting response surface methodology (RSM) is that it provides a scientific basis for identifying critical factors, quantifying variability, and optimizing conditions with reduced testing. This not only enhances accuracy and reliability but also minimizes experimental costs and time, ensuring that the models developed can predict performance under various settings with certainty. Several studies have shown that RSM accuracy can be verified by conducting validation experiments under predicted optimal conditions and comparing experimental results with model predictions using statistical measures [11].

One of the unique characteristics of Harakeke is that it requires a framework capable of accurately modeling the nonlinear relationships between fiber content, raster angle, and raster width to predict machine performance. Furthermore, fiber dispersion and loading are essential for the development of Harakeke-PLA composites into high-performance, eco-friendly materials. Therefore, parameter combinations should prioritize improving stiffness, strength, and interlayer bonding, while aligning with the stability and durability goals required in lightweight structures to enable durable, recyclable applications in the automotive, biomedical, and packaging sectors. By adopting a multi-factor approach, although the tensile and flexural behavior of the composites is a common one, the effects of determining the parameter combinations have not been fully investigated. The difficulty of investigating all the parameters on an experimental basis is realized. By analyzing the effects of various parameter combinations in detail using a limited number of experiments through RSM, it can have a significant impact on future production by identifying the optimal parameters [12,13]. However, the lack of combination parameters in previous studies is felt. This hinders the progress of establishing Harakeke/New Zealand flax PLA composites as high-performance, environmentally friendly, and regionally relevant materials. Although harakeke-reinforced PLA composites hold great promise, the combined effect of raster angle, raster width, and fiber content on mechanical performance has not been systematically investigated, resulting in a significant knowledge gap in the design of high-strength, environmentally friendly 3D-printed composites.

In this work, the tensile and flexural behavior of PLA composites reinforced with Harakeke (New Zealand flax) fiber, produced via FDM 3D printing for lightweight structural applications, is experimentally analyzed. The impact of optimized printing settings on interfacial bonding and overall mechanical performance is highlighted, including fiber content, raster angle, and raster width. The study's unique contribution to the sustainable design of high-strength, lightweight bio composites is highlighted by the development of a predictive RSM model to capture nonlinear effects related to fiber–matrix interactions. Fig. 1 provided a graphical reinforcement mechanism of PLA-New Zealand flax fiber.

Despite the growing body of literature on natural fiber-reinforced PLA composites fabricated via FDM, the use of harakeke (New Zealand flax) fiber as a reinforcement in this context remains largely unexplored. To the best of the authors' knowledge, this is the earliest study

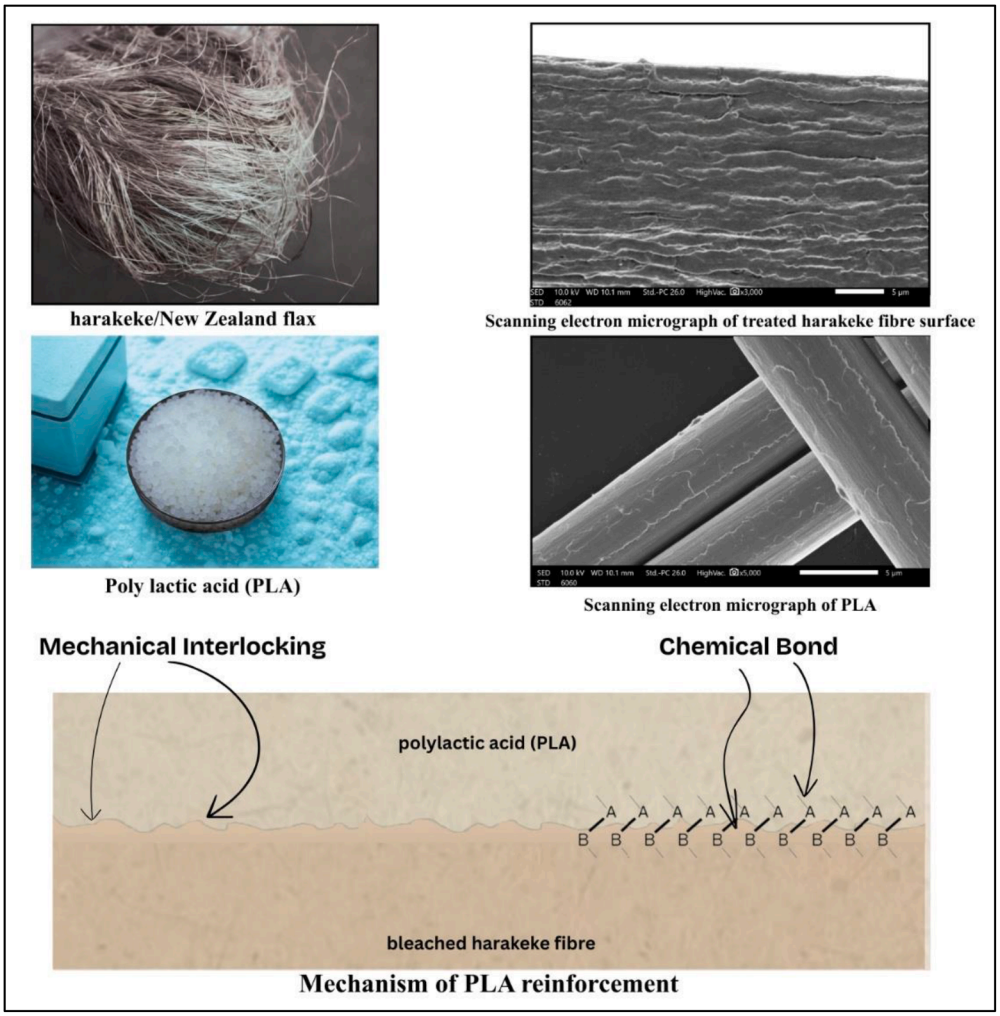

Fig. 1. Graphical reinforcement mechanism of PLA-New Zealand flax fiber.

to systematically investigate the combined effects of harakeke fiber content, raster angle, and raster width on the tensile and flexural performance of FDM-printed PLA composites using a Response Surface Methodology (RSM)-based optimization framework. Unlike prior studies that examine either fiber loading or printing parameters in isolation, this work uniquely integrates both material and process variables within a statistically rigorous multi-factor design, enabling accurate modeling and prediction of mechanical behavior. The cultural significance of harakeke as a regionally important and sustainable fiber further reinforces the environmental and societal relevance of this research.(Table 1).

2. Materials and methods

2.1. Sample preparation

Harakeke fibers, sourced from New Zealand, were harvested from mature leaves measuring 1–1.5 m in length were selected and harvested manually and carefully choose the middle lamina for fiber extraction, the process is consistent and in standard extraction process. These leaves, which are mostly composed of cellulose, hemicellulose, and lignin, and were submitted to two different chemical treatments to improve PLA matrix compatibility. Alkali digestion was performed using sodium hydroxide (NaOH, ≥98%) and sodium sulphite (Na_2SO_3, ≥98%), and peroxide bleaching was carried out using hydrogen peroxide (H_2O_2, 3/90%). The alkali treatment comprised soaking the fibers in a solution of 5% NaOH with 2% Na_2SO_3 at an immersion temperature of 80°C for 2 hours to improve interfacial. Bleach treatment was performed using a 3% H_2O_2 solution at 70°C for 1 hour, followed by extensive rinsing. The removal of lignin and hemicellulose by alkali digestion (5% NaOH + 2% Na_2SO_3 at 80°C for 2 hours) increases the exposure of hydroxyl groups, while peroxide bleaching (3% H_2O_2 at 70°C for 1 hour) further oxidizes surface contaminants, improving fibre polarity and interfacial bonding with PLA. The purpose of these treatments was to remove surface contaminants, increase roughness, and expose hydroxyl groups in cellulose, thereby improving interfacial bonding and adhesion in PLA composites. After being chemically treated, the fibers were mechanically sheared in a TSE-16-TC twin screw extruder at low screw speed of 100rpm at 160 to 180°C temperature range, followed by sunbeam multigrinder with blunt blades, while being run at an elevated speed. To preserve the structural integrity of the Harakeke fibers, a methodical approach was selected to gently shorten and separate them without causing excessive cutting or fibrillation. Blunt-edge high-speed shearing produces uniformly sized fiber pieces with clean surfaces while reducing fiber damage compared to sharp-blade milling. This uniformity enhances the fiber–matrix compatibility and interfacial adhesion by promoting an even distribution within the PLA matrix and facilitating extrusion during FDM processing. Drying harakeke fibers at 105°C for 12 hours and pre-drying PLA are essential to eliminate residual moisture that can induce hydrolytic degradation during FDM processing [28]. Any remaining moisture may cause polymer chain scission, void formation, and poor fiber–matrix adhesion, thereby reducing tensile and flexural performance. The various stages of fiber treatment and sample preparation process is shown in Fig. 2. The bio-based PLA Ingeo Biopolymer 2003D has a specific gravity of 1.24 g/cm^3, a tensile modulus of 3.45 GPa, a tensile strength of 53 MPa, 6% elongation, and a melt flow rate of 6 g/10 min at 210°C [29]. Extrusion and thermoforming are simple methods of processing; nevertheless, drying is necessary to prevent hydrolysis. Although FDM-fabricated harakeke–PLA composites are appropriate for lightweight,

Table 1
FDM fiber composites: parameters, properties, performance, and research gaps.

Author / Year	Fiber Type	Fiber Treatment	FDM Parameters Considered	Key Mechanical Findings	Major Limitations / Gaps
[14]	Jute, Flax, Sisal	Alkali, Silane	Raster angle, infill, layer thickness	Improved tensile/flexural strength vs. neat PLA; best with alkali/silane treatment	Anisotropy, voids, limited interfacial bonding
	Hemp, Flax	Alkali	Layer height, infill, orientation	Hemp-PLA comparable to CF-PLA in impact/compression; lower tensile than CF	Lower tensile than CF, interlayer adhesion issues
	Wood Fiber	Untreated	Layer height, infill, orientation	Enhanced mechanical/sustainability, improved modulus	Lower strength than CF, voids
[15]	Wood Fiber	Untreated	Layer height, infill density	+18% tensile, +22% flexural vs. PLA; higher energy absorption	Lower tensile/stiffness than neat PLA, water absorption
[16]	Banana Fiber	Untreated	Nozzle size, infill, layer thickness	Max tensile ~32 MPa, flexural ~151 MPa at 3% fiber	Limited fiber content range, nozzle clogging at high load
[17]	Flax	Alkali, Silane	Not specified	+60% fracture toughness/strain energy release rate	Not all treatments scalable, limited FDM focus
[18]	Kenaf	NaOCl, NaOH	Not specified	NaOCl best for lignin/hemicellulose removal, improved bonding	Not directly FDM, limited mechanical data
[19]	Wood Fiber	Untreated	Fiber size, infill, layer thickness	≤100 μm fibers: improved tensile/flexural, better printability	Agglomeration at high content, nozzle clogging
[20]	Banana Fiber	Untreated	Nozzle size, infill, layer thickness	Zig-zag infill, 3% fiber: +70% impact strength vs. PLA	Only low fiber content, limited durability data
[21]	Pineapple Leaf	Untreated	Infill density, layer thickness	60–100% infill: improved tensile/fatigue, good fiber-matrix interaction	High infill increases weight, limited fiber treatment
[22]	Carbon Fiber	Untreated	Layer height, infill, orientation	+30–40% tensile/flexural vs. PLA, best at 5–20% CF	Reduced flexural at high CF, not biodegradable
[23]	Wood Fiber	Untreated	Print orientation	X-orientation: highest tensile/impact; Z: weakest due to interlayer bonding	Strong anisotropy, orientation-dependent
[24]	Jute, Flax, Sisal	Alkali, Silane	Not specified	Improved strength, moisture/UV resistance, toughness	Limited FDM studies, interface optimization needed
[25]	Wood Fiber	Untreated	Infill, layer height, orientation	ML models (XGBoost) accurately predict tensile/failure strain	Model generalizability, limited experimental validation
[26]	Carbon black	Untreated	Nozzle temperature, bed temperature, fan speed	Optimal parameters (220°C, 45°C, 85%) improved tensile strength (26.37 MPa), modulus (~825 MPa), and strain energy density; strong statistical significance of thermal parameters	Optimal parameters (220°C, 45°C, 85%) improved tensile strength (26.37 MPa), modulus (~825 MPa), and strain energy density; strong statistical significance of thermal parameters
[27]	Conductive fillers (likely carbon-based, TPU matrix)	Conductive fillers (likely carbon-based, TPU matrix)	Conductive fillers (likely carbon-based, TPU matrix)	Conductive fillers (likely carbon-based, TPU matrix)	Conductive fillers (likely carbon-based, TPU matrix)

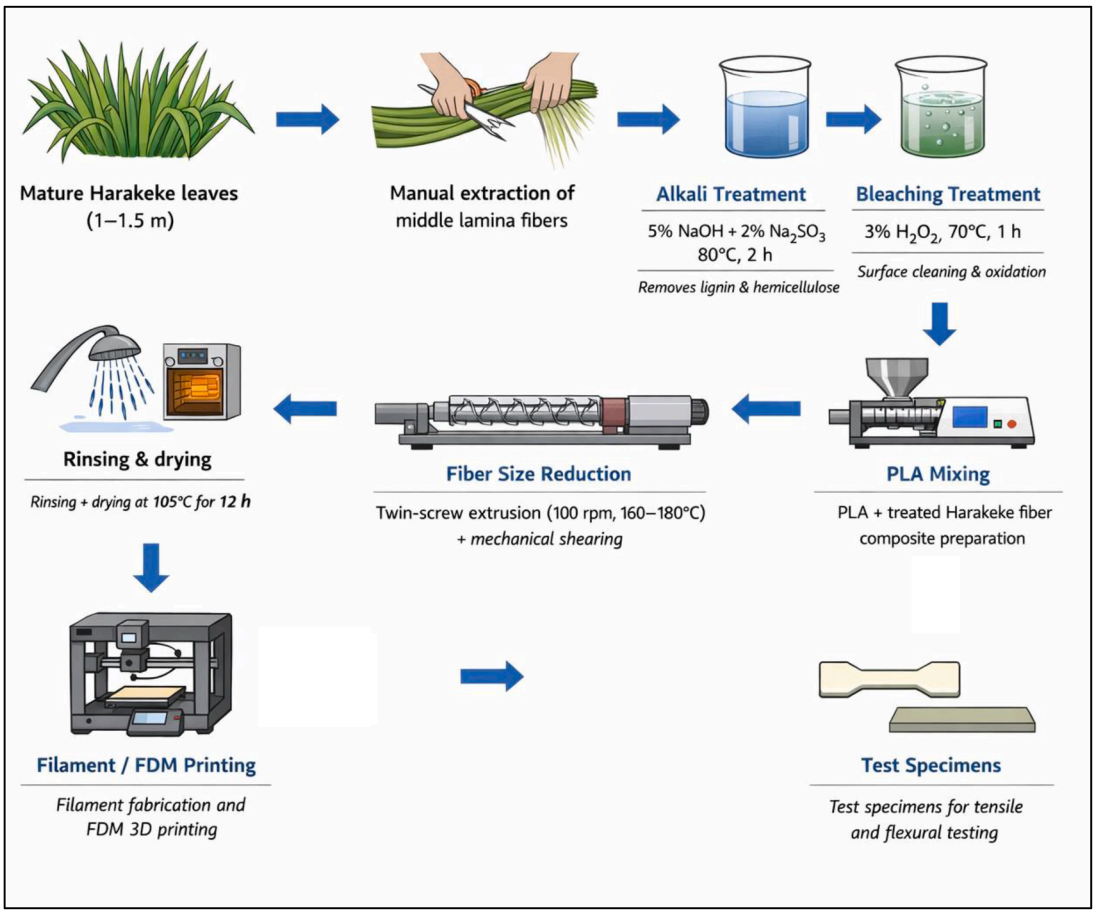

Fig. 2. Sample preparation process.

environmentally friendly components, their use in thermally demanding applications is limited by their low heat distortion temperature (55°C), which can result in slight warping or dimensional instability during cooling or exposure to high service temperatures.

Test specimens were fabricated using fused deposition modelling (FDM) on a 3D printer, which was conFig.d with a melting zone of 190–210°C and a nozzle temperature of 200°C. A controlled cooling period followed to ensure dimensional stability and solidification [30]. Composites were coded as "PLA" for neat PLA and "PLA + FF X" for flax fiber composites, where X denotes the fiber weight percentage. This systematic approach, from fiber treatment and PLA drying to extrusion and FDM, ensured the production of high-quality, reproducible specimens, facilitating the evaluation of fiber content and treatment effects on composite performance. Among the various processing parameters identified in this study, due to their significant impact on fiber orientation, load transfer, and interlayer bonding, the three parameters flax infill percentage, raster angle, and raster width were given priority. To isolate their effects and guarantee a controlled assessment of mechanical performance, other elements were kept constant, as detailed in Table 2.

2.2. Experimental parameters setting using DOE

Experimental parameters were determined using Design of Experiment (DOE), a statistical program designed for experimental design. The Central Composite Design (CCD) method was employed in this investigation, which included three repetitions at the central point. CCD reduces the number of experimental runs compared to full factorial designs. raster angle (A), raster width (B), and fibre density (C) were selected as independent variables. This is based on their known influence on fiber orientation, interlayer bonding and load transfer. The parameters of the Central composite design for this test are presented in Table 3.

Six repetitions were added to the center point to improve experimental reliability. This allowed for precise measurement of experimental error and evaluation of model suitability for both tensile and flexural testing. Twenty experimental runs were conducted using the CCD framework, which ensured adequate coverage of linear, quadratic, and interaction effects while achieving an ideal balance between statistical rigor and experimental efficiency. Crucially, both tensile and flexural tests were conducted using the CCD-derived input parameters consistently, preserving consistent testing conditions and enabling a

Table 2
Printing parameters.

Material:	Polylactic acid (PLA) reinforced with flax fibres
Infill Pattern:	Rectilinear
Filament Diameter:	1.75 ± 0.10 mm.
Print Head Travel Speed:	30 mm/s.
Nozzle Temperature:	200°C
Nozzle Diameter:	0.75 mm
Bed Temperature:	70°C.

Table 3
Amounts and ranges of parameters in central-composite design.

Parameters	Factors	Symbol	Levels		
			-1	0	1
Raster Angle (°)	A	X_1	45	60	90
Raster Width (mm)	B	X_2	0.5	0.75	1
Fiber Density (wt.%)	C	X_3	0	10	20

direct comparison of the mechanical performance of the various composite specimens. Based on the CCD design, a total of 20 samples were recommended. The number of runs of the CCD directed design is presented in Table 4.

2.3. Tensile test

In accordance with ASTM D638 standards, PLA/New Zealand flax composite specimens were subjected to tensile and flexural testing utilizing an Instron Bluehill 3369 universal testing equipment . To achieve consistent mechanical behavior and homogeneous moisture content, Type-1 specimens were 3D printed to standard dimensions and then conditioned for 48 hours at 24°C and 50% relative humidity in a climate room. A computerized caliper was used to measure the initial geometrical parameters, ensuring precise stress calculations and repeatability of the tensile and flexural results. In order to reduce eccentricity effects and guarantee consistent force application along the specimen axis, a 5 kN load cell was used in conjunction with correctly aligned grips. The crosshead speed for tensile testing was selected in accordance with ASTM D638 to maintain standardized strain rates, allowing valid comparison of mechanical properties. Real-time stress–strain data were recorded via the Bluehill software to determine critical mechanical characteristics, including tensile strength, yield strength, elongation at break, and elastic modulus. A schematic diagram of the tensile test specimen is presented in Fig. 3.

2.4. Flexural test

For flexural evaluation, a three-point loading fixture was mounted, and the specimens were placed with two bearing points and a suitable span length, which was determined in relation to thickness. A 5 KN load cell was used, and the crosshead speed was set at 1 mm/min according to ASTM D790 [31]. According to ASTM D790 standard, the test specimens used here have a cross-section of 3.2 mm x 12.7 mm and a length of 125 mm. The specified thickness-to-support ratio of 16 results in a support span of 51 mm. Force-deflection data were recorded in real time; stress-strain curves were provided for flexural strength, flexural modulus, and maximum displacement. Post-testing analysis included verifying compliance with their respective ASTM standards, assessing failure modes, and validating the data. Repeatability, reliability, and precision have been verified through testing multiple specimens under the same conditions. Flexural test specimen details are presented in Fig. 4.

Table 4
3D printing processing parameters of composites for 20 runs based on CCD design.

Run/Sample Number	Code values			A: Raster Angle (°)	B: Raster Width (mm)	C: Fiber Content (wt%)
	X_1	X_2	X_3			
1	-1	-1	-1	45	0.5	0
2	1	-1	-1	90	0.5	0
3	-1	1	-1	45	1.0	0
4	1	1	-1	90	1.0	0
5	-1	-1	1	45	0.5	20
6	1	-1	1	90	0.5	20
7	-1	1	1	45	1.0	20
8	1	1	1	90	1.0	20
9	-1	0	0	45	0.75	10
10	1	0	0	90	0.75	10
11	0	-1	0	60	0.5	10
12	0	1	0	60	1.0	10
13	0	0	-1	60	0.75	0
14	0	0	1	60	0.75	20
15	0	0	0	60	0.75	10
16	0	0	0	60	0.75	10
17	0	0	0	60	0.75	10
18	0	0	0	60	0.75	10
19	0	0	0	60	0.75	10
20	0	0	0	60	0.75	10

2.5. Optimization by RSM

Response Surface Methodology (RSM) was employed to optimize the process parameters and identify the optimal combination of raster Angle, raster width, and fiber density for achieving superior mechanical performance [32,33]. The experimental data from CCD were regressed against a second-order polynomial model, and three-dimensional response surface plots were created to see the interaction between factors and responses. This second-order polynomial model enhances RSM regression accuracy by representing both linear and nonlinear relationships between process parameters, as well as providing accurate predictions of the optimal additives for Harakeke-PLA blends. The optimization was performed to maximize flexural strength, Young's modulus, and tensile strength, while minimizing strain and displacement. The desirability function analysis was used to optimize the multiple response variables, considering the judicious trade-off between conflicting objectives. This method yielded the best parameter values, demonstrating statistical reliability and real-world applicability. The research provides important insights into the mechanical properties of bio-based composites by investigating the tensile and flexural performance of eco-friendly green flax-PLA composites 3D printed. Three-dimensional response surface plots graphically depict the interaction between raster angle, raster width, and fiber density, visually showing synergistic or antagonistic effects on tensile and flexural performance. Such plots help determine the area where the combined effect of parameters yields maximum mechanical strength and overall composite performance.

3. Results and discussions

3.1. Tensile test results

Tensile testing of PLA–flax composites was conducted based on the DOE's Central Composite Design (CCD), allowing systematic analysis of raster angle (A), raster width (B), and fibre density (C) at multiple levels to identify both linear and interaction effects. The CCD approach enabled the determination of optimal parameter settings with reduced experimental runs and increased statistical reliability. The highest Young's Modulus of 4728.12 MPa was found for the specimen "PLA flax 20%-7" (Raster Width: 1 mm, Raster Angle: 45°, Fiber Density: 20 wt.%), confirming that 45° raster orientation improves stiffness uniformly over 90° by ensuring effective load transfer along diagonal fiber directions. Conversely, the highest Ultimate Tensile Stress of 49.06 MPa was realized for specimen "PLA flax 0%-3" (Raster Width: 1 mm, Raster Angle: 45°, Fiber Density: 0 wt.%), suggesting that reduced flax infill supports increased tensile strength. Raster width had a relatively minor impact on tensile performance because changes in filament spacing had a negligible effect on interlayer fusion compared to the dominating impacts of fibre density and raster angle on failure behavior and stress distribution. Due to inadequate fiber–matrix adhesion, increasing the flax percentage decreased tensile strength and ductility while simultaneously increasing stiffness through increased fiber reinforcing. Pure PLA prints feature unbroken polymer chains, enhanced interlayer bonding, reduced melt viscosity, and fewer voids or stress-concentrating areas. Inclusion of flax raises melt viscosity and may lead to fiber agglomeration, bad wetting, micro voids, and weak fiber–matrix interfaces (fiber pull-out or breakage), all decreasing effective load transfer and reducing UTS. In our tests, the best stiffness–strength balance was found at low flax loadings (10 wt.%). However, increasing fibre content introduced defects during processing and at the interface, which lowered the tensile strength compared to neat PLA. Table 5 represents the tensile test responses of PLA–flax composites based on RSM experimental design.

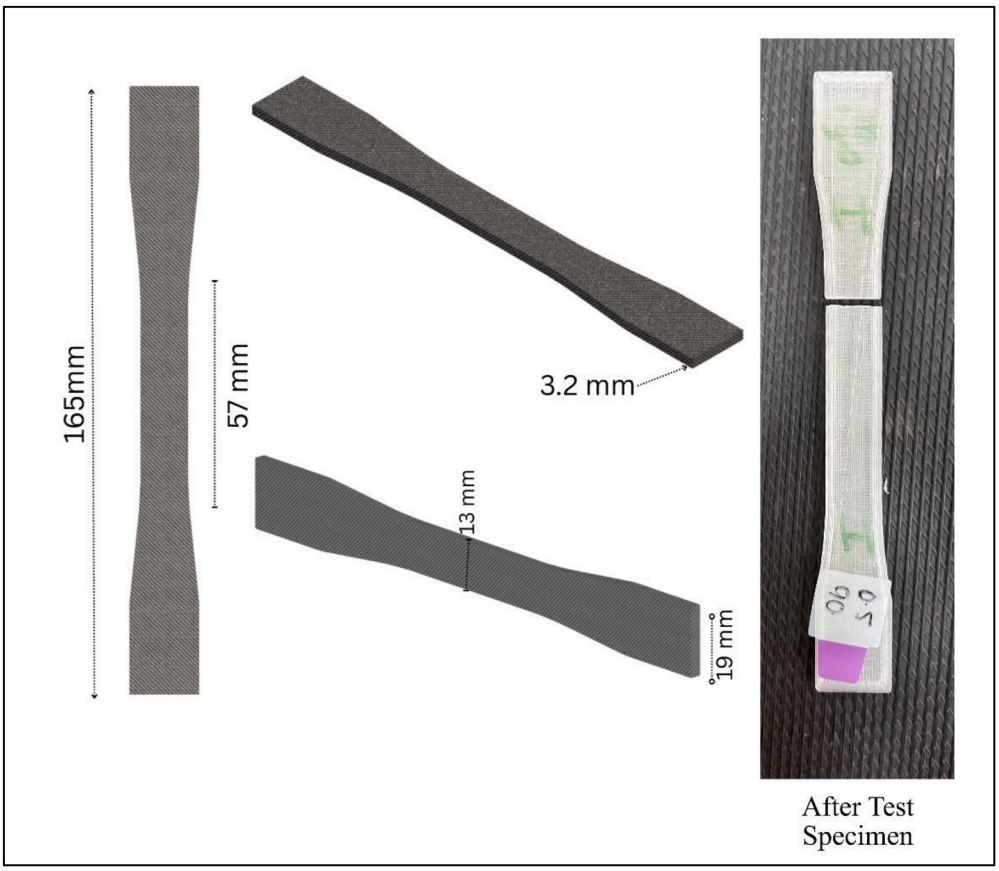

Fig. 3. Schematic diagram of tensile test specimen.

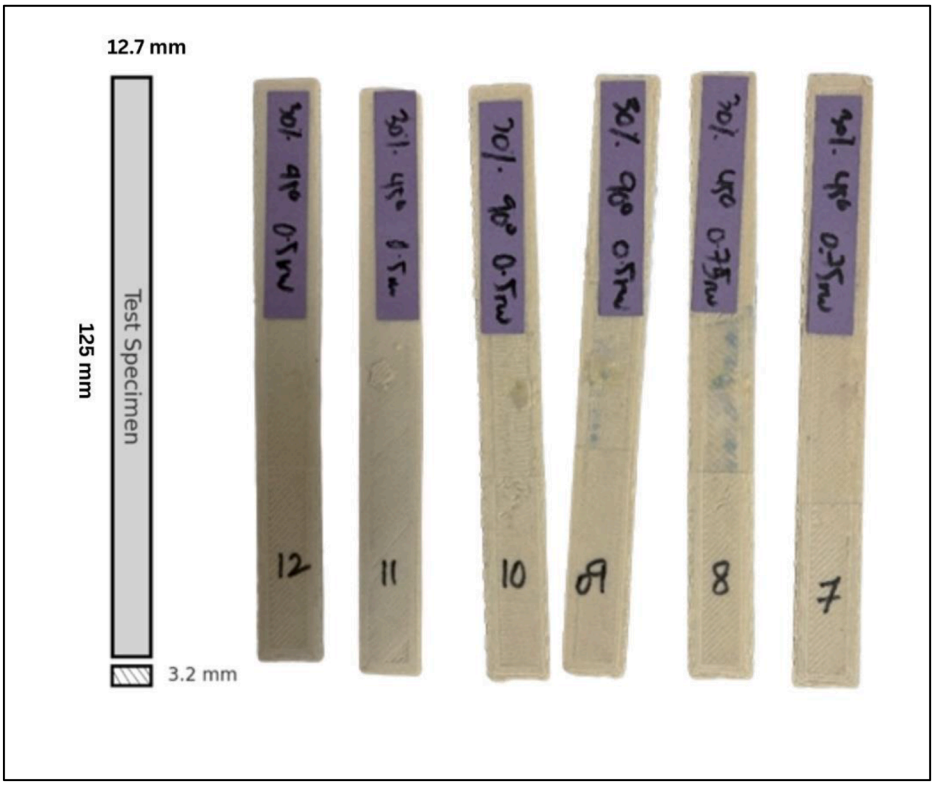

Fig. 4. Flexural test specimen details.

Table 5
Tensile test responses of PLA–flax composites based on RSM experimental design.

Run	Factor 1 A: Raster Angle (degree)	Factor 2 B: Raster Width (mm)	Factor 3 C: Fibre (%)	Response 1 Young's Modulus (MPa)	Response 2 Ultimate Tensile Stress (MPa)	Response 3 Tensile Stress at Break (MPa)	Response 4 Displacement at Break (mm)	Response 5 Tensile Strain (%)
1	45	0.5	0	3844.43	43.69	23.61	3.19	1.91
2	90	0.5	0	4171.57	48.37	37.12	2.77	1.66
3	45	1	0	4040.82	49.06	25.1	3.68	2.20
4	90	1	0	4057.22	42.91	24.63	2.35	1.41
5	45	0.5	20	3662.18	42.91	23.33	2.96	1.77
6	90	0.5	20	3659.41	37.08	29.75	2.12	1.27
7	45	1	20	4728.12	43.33	23.5	2.67	1.62
8	90	1	20	4413.27	35.13	19.74	2.11	1.28
9	45	0.75	10	4580.57	40.63	21.69	2.56	1.55
10	90	0.75	10	4038.84	32	18.31	2.38	1.44
11	60	0.5	10	4470.7	38.91	28.73	2.71	1.64
12	60	1	10	4312.96	36.25	19.31	2.59	1.57
13	60	0.75	0	4412.49	36.36	20.4	2.55	1.31
14	60	0.75	20	3951.49	28.72	22.11	2.28	1.21
15	60	0.75	10	4279.99	33.74	19.49	2.57	1.39
16	60	0.75	10	3714.88	27.33	15.21	2.25	1.24
17	60	0.75	10	4150.66	31.12	30.81	2.21	1.26
18	60	0.75	10	3257.33	22.63	17.57	2.25	1.14
19	60	0.75	10	3267.33	25.63	19.57	2.13	1.13
20	60	0.75	10	3249.33	24.63	16.57	2.31	1.21

3.1.1. Influence of flax infill content on tensile properties

Generally, increasing flax infill enhances the composite's stiffness, as reflected by higher Young's Modulus values due to improved load transfer between fibers and the PLA matrix. The maximum Young's Modulus of 4728.12 MPa was found at 20 wt.% flax (0.5 mm, 45°), which shows efficient reinforcement, but a decrease from that at 10 wt. % flax implies fiber agglomeration and inhomogeneous dispersion at increased loadings, which will prevent stress transfer and enhance melt viscosity upon processing. Ultimate Tensile Stress (49.06 MPa) was the highest in pure PLA (0 wt.% flax, 0.75 mm, 45°), where the uniform polymer matrix remained continuous and did not experience fiber-induced discontinuities. Incorporation of flax fibers created local concentrations of stress and poor interfacial zones, decreasing both Ultimate Tensile Stress and Tensile Stress at Break (up to a maximum of 37.12 MPa at 0 wt.% flax, 0.5 mm, 90°). As the flax content increased, displacement and strain decreased, indicating lower ductility and greater brittleness resulting from the fiber–matrix stiffness. The 30 wt.% flax confirmation run demonstrated higher contrast effects, resulting in overloading of the fibers, which led to aggregation, decreased polymer flow, and degraded interfacial bonding, supporting the negative effect of over-reinforcement on overall tensile behavior. Similar reductions in mechanical properties due to fiber agglomeration and weak interfacial bonding in natural fiber-reinforced PLA composites have been reported in earlier studies. A total of 20 specimens were tested according to the CCD matrix, along with six additional confirmation runs conducted to validate the optimized process parameters and ensure reproducibility. Fig. 5 provides an overview of the Influence of flax infill density on various responses.

3.1.2. Influence of raster angle on tensile properties

Specimens with a 45° raster angle consistently exhibit higher Young's Modulus than those with a 90° angle across all flax percentages due to better load distribution along diagonal fiber orientations. Fig. 6 provides Young's Modulus vs Raster Angle at 0.5,0.75,1.0 mm raster widths.

The 45° angle generally yields higher Ultimate Tensile Stress. The 45° angle improves strength, with the highest stress (49.06 MPa) observed at 0% flax, 0.75 mm, and 45°, indicating a better fiber-matrix interaction at this orientation. Fig. 7 represents the ultimate tensile stress vs raster angle at 0.5,0.75, and 1.0mm raster widths.

The 45° angle slightly improves stress and strain at break, indicating marginally better ductility and toughness.

3.1.3. Influence of raster width on tensile properties

Raster width has a less pronounced effect, but 0.5 mm tends to yield higher modulus values. Smaller raster widths (0.5 mm) correlate with higher stiffness, possibly due to denser material deposition; however, the effect is less significant than that of flax infill or angle. Fig. 8 represents the Young's modulus vs. raster width at 45° and 90° raster angles.

The 0.75 mm raster width achieves the highest Ultimate Tensile Stress (49.06 MPa at 0% flax, 45°), but differences are small, suggesting raster width has a minor influence on strength. Fig. 9 represents the ultimate stress versus raster width at 45 ° and 90° raster angles.

3.1.4. Relationships and correlations

The experimental data analysis reveals strong interdependencies between raster angle, raster width, and fiber density in determining the final mechanical properties. Young's modulus generally increases with higher raster angles (e.g., 90° and 45°), with the highest value of 4728.12 MPa observed at a 45° raster angle, a width of 1 mm, and a fiber density of 20 wt.%. Ultimate tensile stress also exhibited the same trend, with greater values observed at lower fiber contents, and a significant decrease resulting from excessive fiber addition (20 wt.%), reflecting poor matrix–fiber bonding. Tensile stress at break and break displacement were negatively correlated with fiber density, where an increased content of flax decreased ductility and the capacity for strain. Runs with moderate fiber density (10 wt.%) and intermediate raster levels showed balanced mechanical performance, indicating an optimal compromise between toughness and stiffness. The correlations identify that raster angle significantly controls stiffness, raster width controls load distribution, and fiber density significantly influences ductility, such that over-reinforcement causes deterioration of performance.

The results were quantitatively compared with earlier studies on PLA–natural fibre FDM composites. The highest Young's Modulus in this study, 4728.12 MPa (45° raster angle, 20 wt.% flax, 1 mm width), falls within the reported range (3800–4500 MPa), indicating a 5–24% increase in stiffness. This improvement is consistent with the literature, which indicates that a 45° raster angle yields a more uniform stress distribution and better load transfer between layers than 0°/90° orientations. The highest Ultimate Tensile Stress of 49.06 MPa (0 wt.% flax, 45°, 1 mm) is little higher than many other values (35–45 MPa) that have been reported [34,35]. Additionally, the lower tensile strength with increased fiber content (20 wt.%), which coincides with previous research, can be explained by fiber aggregation, inadequate wetting, and

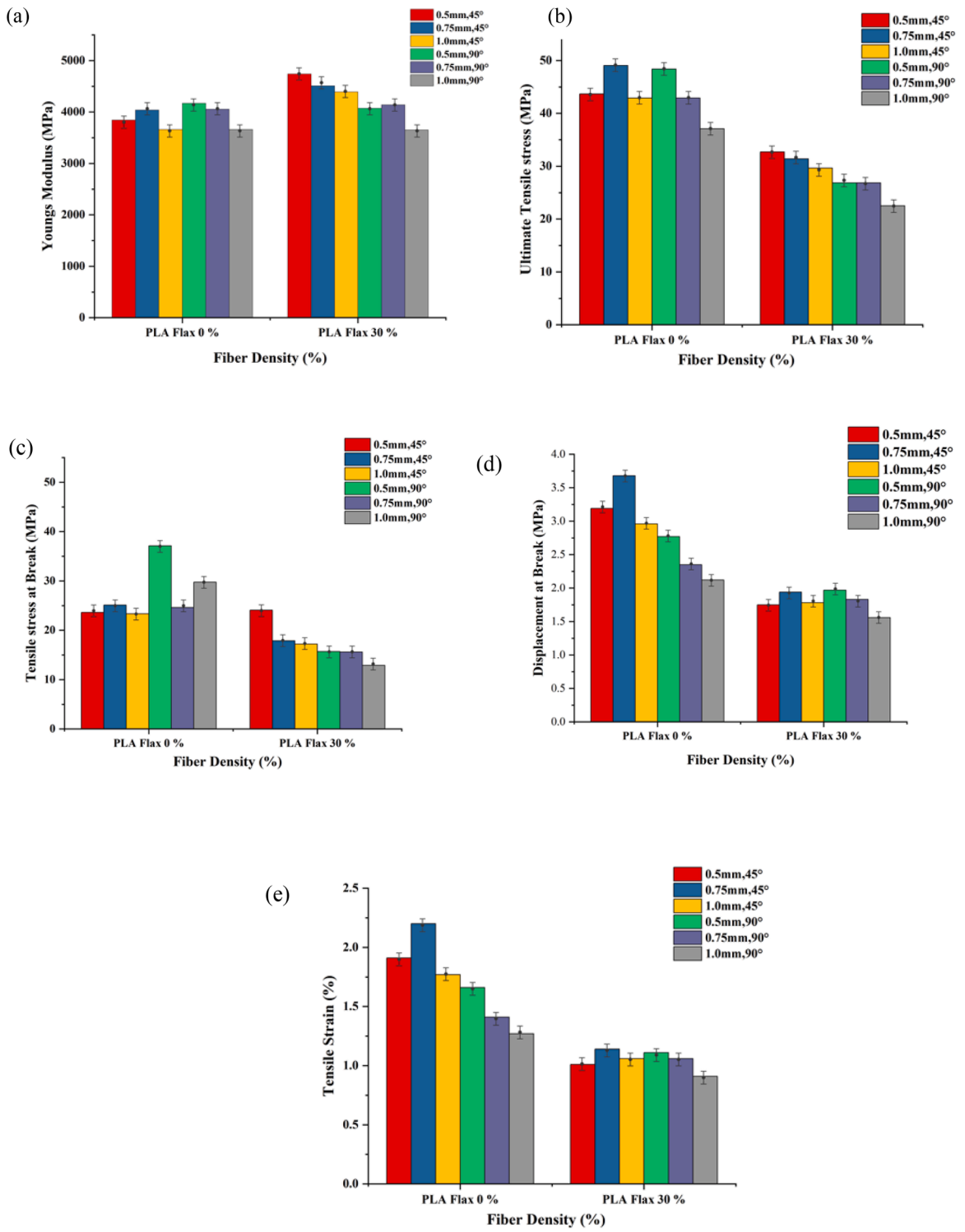

Fig. 5. Influence of flax infill density: (a) Young's Modulus, (b) Ultimate Tensile stress, (c) Tensile stress at Break, (d)Displacement at Break, (e) Tensile strain.

poor interface bonding that lead to ineffective stress transfer. This research confirms that mechanical properties depend on both raster-induced anisotropy and fiber dispersion processes mentioned in past literature [22].

3.2. Flexure test results

Table 6 represents the flexural test responses of PLA–flax composites based on RSM experimental design. The highest Young's Modulus (4453.85 MPa) and flexural stress (73.395 MPa) were observed for the composite with 10 wt.% flax infill, 0.5 mm raster width, and 45° raster angle, indicating an optimal balance between fiber reinforcement and matrix integrity.

This peak performance suggests effective fiber-matrix stress transfer at 10 wt.% flax, facilitated by the excellent printability of the composites, particularly those with bleached and sonicated fibers, which enabled uniform extrusion without nozzle clogging even at high fiber loadings. However, both modulus and flexure stress decreased

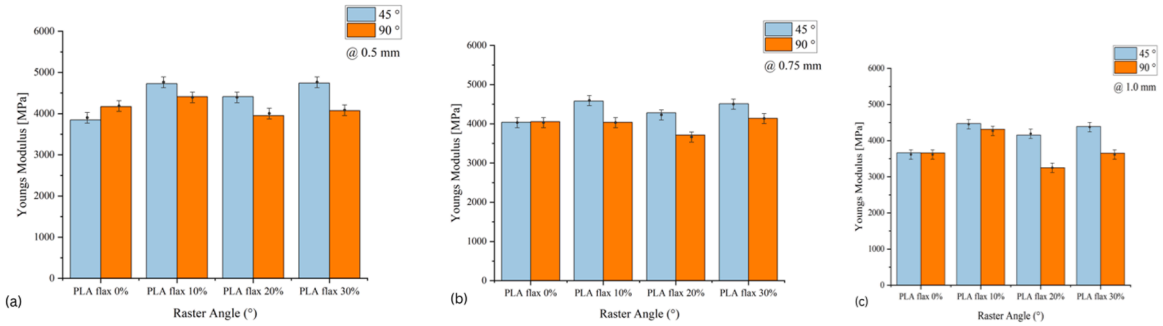

Fig. 6. (a), (b), (c): Young's modulus vs raster angle at 0.5, 0.75, and 1.0 mm raster widths.

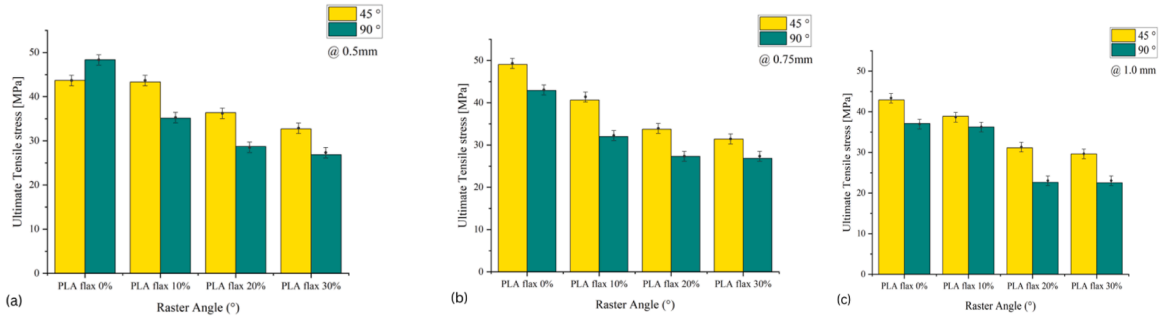

Fig. 7. (a), (b), (c): Ultimate tensile stress vs raster angle at 0.5, 0.75, and 1.0 mm raster widths.

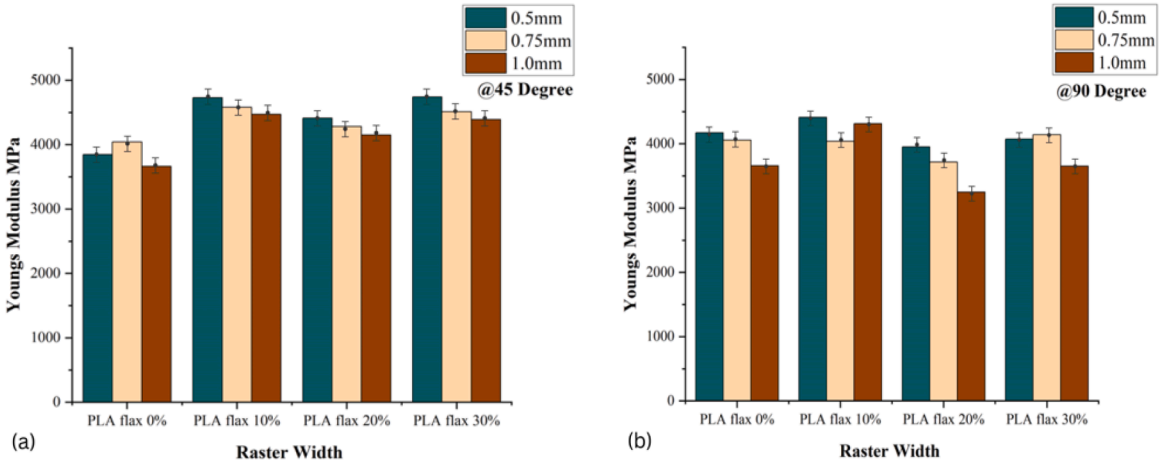

Fig. 8. (a), (b): Young's modulus vs raster width at 45°, and 90° raster angles.

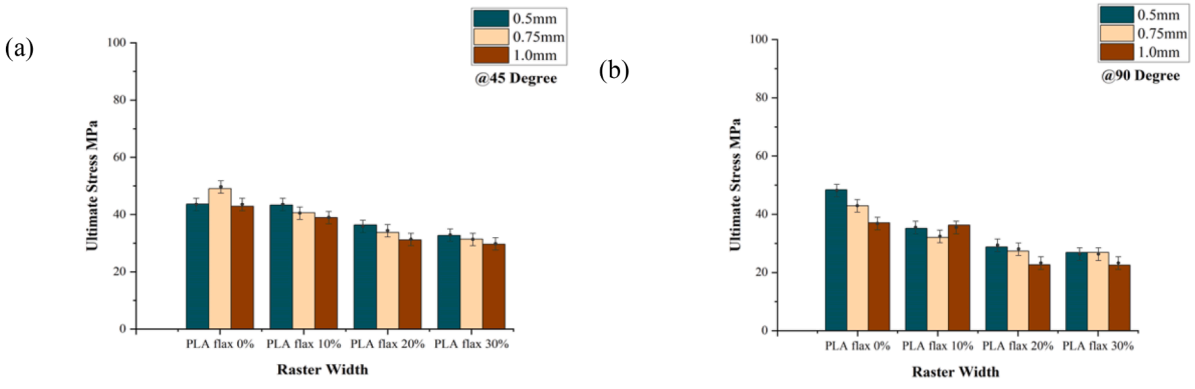

Fig. 9. (a), (b): Ultimate stress vs raster width at 45° and 90° raster angles.

Table 6
Flexural test responses of PLA–flax composites based on RSM experimental design.

Run	Factor 1 A: Raster Angle (°)	Factor 2 B: Raster Width (mm)	Factor 3 C: Fibre Density (wt. %)	Response 1 Flexure Strain (%)	Response 2 Flexure Stress (MPa)	Response 3 Flexure displacement (mm)	Response 4 Young's Modulus (MPa)
1	45	0.5	0	1.79	69.47	2.33	4077.20
2	90	0.5	0	1.735	66.70	2.26	4065.93
3	45	1	0	1.72	63.765	2.24	3871.21
4	90	1	0	1.75	62.215	2.275	3782.92
5	45	0.5	20	1.585	43.21	2.065	3112.43
6	90	0.5	20	1.65	42.41	2.15	2970.74
7	45	1	20	1.805	48.23	2.35	3196.80
8	90	1	20	1.63	37.635	2.13	2609.42
9	45	0.75	10	1.895	68.16	2.475	3949.25
10	90	0.75	10	1.825	64.095	2.375	3960.99
11	60	0.5	10	1.86	66.0	2.40	4010.00
12	60	1	10	1.78	62.0	2.30	3850.00
13	60	0.75	0	1.76	65.5	2.28	3970.00
14	60	0.75	20	1.70	41.0	2.20	2900.00
15	60	0.75	10	1.85	66.5	2.42	3950.00
16	60	0.75	10	1.84	66.2	2.40	3965.00
17	60	0.75	10	1.86	66.8	2.41	3975.00
18	60	0.75	10	1.85	66.4	2.39	3960.00
19	60	0.75	10	1.87	67.0	2.43	3980.00
20	60	0.75	10	1.86	66.6	2.41	3970.00

significantly at higher flax infill densities (20%), with averages of 3100.80 MPa for Young's modulus and 45.36 MPa for stress, respectively. This decline likely results from fiber agglomeration or an increase in the viscosity of the molten composite, which can disrupt uniform fiber dispersion, despite the absence of printing issues reported in this experiment.

3.2.1. *Influence of Raster Angle on Flexural Properties*

The raster angle had a significant influence on mechanical performance. Composites printed with a 45° raster angle exhibited a higher average modulus (3606.99 MPa) compared to those at 90° (3265.42 MPa), representing an increase of approximately 341 MPa. Similarly, flexure stress was higher at 45° (average 57.21 MPa) than at 90° (51.37 MPa). This trend suggests that a diagonal fiber orientation of 45° enhances load distribution under flexural loading, thereby improving stiffness and strength. The consistency of this finding with tensile test data reported elsewhere indicates that raster angle is a critical parameter for optimizing mechanical properties in 3D-printed composites.

3.2.2. *Influence of Raster Width on Flexural Properties*

Raster width also affected flexural properties, with smaller widths (0.5–0.75 mm) generally yielding superior performance. The 0.5mm raster width achieved the highest modulus (4453.85 MPa at 10 wt.% flax, 45°), while the 0.75 mm width showed the highest average modulus (3670.94 MPa). In contrast, the 1.0 mm raster width yielded the lowest average modulus (3,192.07 MPa) and flexural stress (48.37

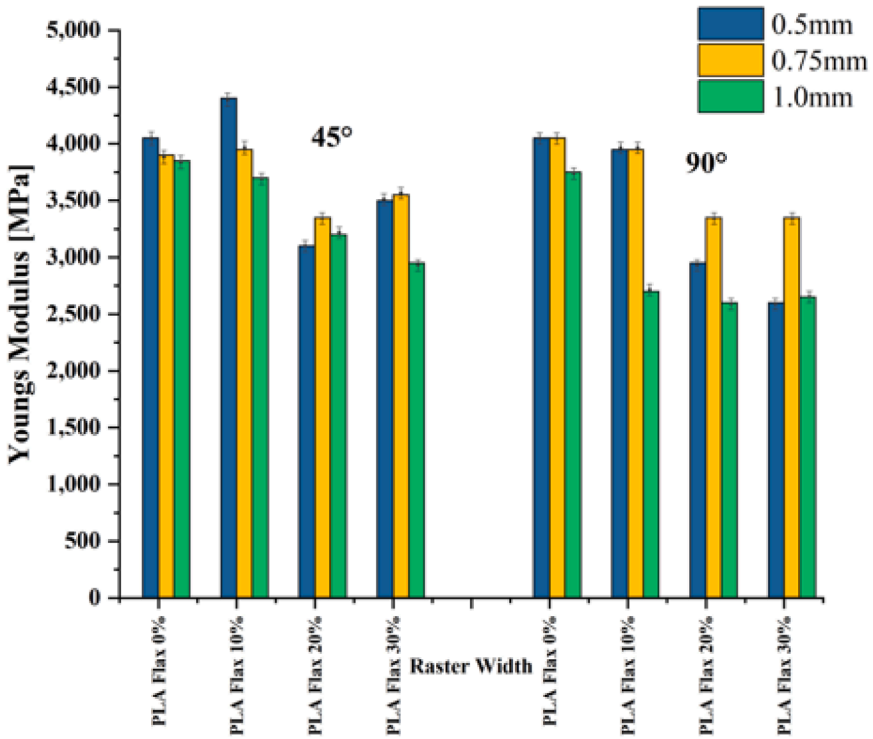

Fig. 10. Youngs Modulus vs Raster width at 45°,90° raster angle (flexural).

MPa). These results suggest that smaller raster widths enable denser material deposition, enhancing fiber-matrix interactions and mechanical properties, particularly when combined with optimal flax infill and raster angle. Youngs modulus vs Raster width at 45°,90° raster angle (flexural) is presented in Fig. 10.

Flexure strain and displacement at tensile strength showed minimal variation across flax infill density, with averages ranging from 1.69% to 1.81% for strain and 2.21 mm to 2.36 mm for displacement. The highest values (1.90% strain and 2.48 mm displacement) occurred at 10 wt.% flax (1.0 mm, 45°), indicating slightly enhanced ductility at this infill level. The stability of these properties suggests that flax addition does not significantly compromise ductility under flexural loading, likely due to the robust printability achieved with consistent printing parameters, as noted in the successful application of neat PLA settings across all composites. Fig. 11 represents the flexural stress vs raster width at 45° and 90° raster angles.

A non-linear relationship was observed between Young's modulus and flax infill density, with a peak at 10 wt.% (4453.85 MPa) followed by a decline at 20 wt.%. This suggests optimal fiber content for stiffness, with higher loadings potentially causing fiber clustering or viscosity-related processing challenges, which can be mitigated using bleached and sonicated fibers that ensure uniform extrusion. Flexure stress exhibited a negative correlation with flax infill, decreasing from 65.50 MPa (0 wt.% average) to 44.38 MPa (20 wt.% average), indicating that excessive fiber content may introduce stress concentrations. The 45° raster angle consistently enhanced modulus and stress, underscoring the importance of fiber orientation. No significant correlation was observed between flexure strain or displacement and flax infill, suggesting that ductility was maintained. Parameter interactions revealed that the combination of 10 wt.% flax, 0.5 mm raster width, and 45° angle optimized mechanical performance, highlighting a trade-off between stiffness and strength at higher flax loadings. The ability to print all composites, including those with 20 wt.% flax, using appropriate PLA parameters without nozzle clogging is noteworthy. The use of bleached and sonicated fibers likely minimizes viscosity-related issues, ensuring uniform filament extrusion and consistent mechanical properties. This robust printability supports the observed trends, particularly the high performance at 10 wt.% flax, and suggests that processing advancements can mitigate challenges associated with high fiber loadings. The reduction in mechanical properties observed at high fiber loadings in natural fiber–PLA composites is attributed to common phenomena such as fiber agglomeration, insufficient wetting, and void formation.

Homogeneous nature of pure PLA results in its high tensile strength since the polymer matrix of PLA can conduct mechanical stresses without breaks due to its homogeneous and continuous structure. Since there are no fibers, the defects such as voids, agglomerations, and weak interface zones are reduced resulting in higher tensile strength. As for the addition of flax fibers, they increase the Young's modulus as they are inherently stiff, which means that their presence will hinder the movements of the polymer chains, thus, providing greater stiffness. However, exceeding the limit of 10% by weight of fibers in the composition causes decreasing of the tensile strength due to poor adhesion of the fibers and the matrix, increased melt viscosity, agglomeration of the fibers, and accumulation of stresses.

The investigation of the flexural properties of 3D-printed PLA-flax composites reveals that flax infill density, raster width, and raster angle significantly influence mechanical performance. An optimal flax infill of 10 wt.%, combined with a 0.5 mm raster width and 45° raster angle, maximizes Young's Modulus (4453.85 MPa) and flexural stress (73.395 MPa), indicating an effective balance of fiber reinforcement and matrix integrity. Higher flax loadings (20 wt.%) reduce the modulus and stress, likely due to fiber agglomeration or increased viscosity. However, the use of bleached and sonicated fibers enabled successful printing without nozzle clogging, ensuring process reliability. The 45° raster angle consistently enhances stiffness and strength compared to 90°, reflecting improved load distribution. Meanwhile, smaller raster widths (0.5–0.75 mm) favor higher mechanical properties. These findings highlight the importance of optimizing fiber content and printing parameters to achieve superior flexural performance in PLA-flax composites for structural applications.

Failure mechanism of the PLA-flax composite were elucidated in light of mechanical performance and structure-process correlations. The neat PLA displayed high tensile strength owing to its continuous polymeric matrix, allowing even stress distribution and delayed crack

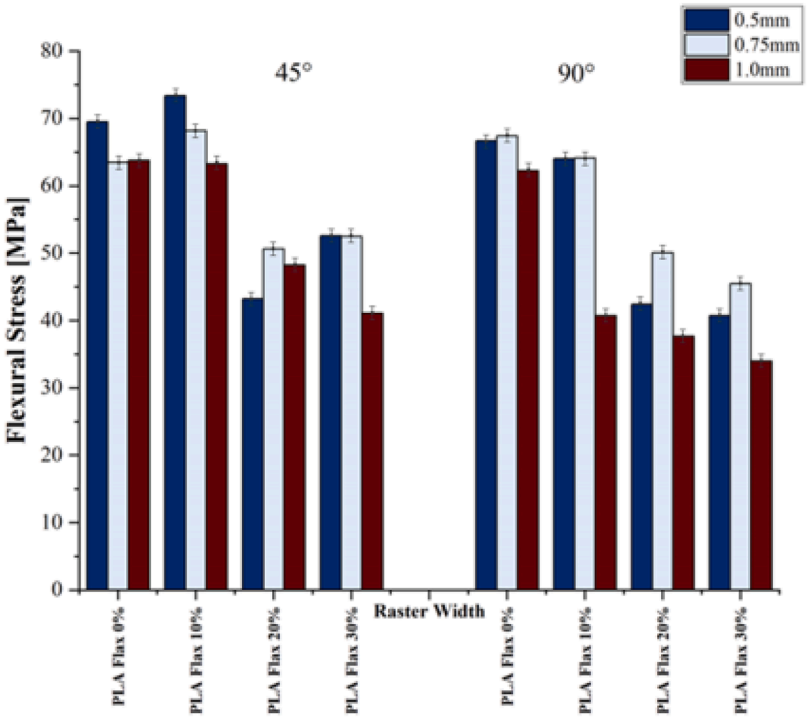

Fig. 11. Flexural Stress vs Raster width at 45°, and 90° raster angle.

propagation. On the other hand, composites with flax reinforcement had low tensile strength at high fiber content due to poor fiber-matrix interface bonding, fiber agglomeration, and high voids during extrusion. These flaws acted as stress concentrators and caused early failure. At the optimum fiber content of 10 wt.%, effective fiber-to-matrix load transfer enhanced stiffness but retained good strength levels. Furthermore, the raster angle greatly affects the path of crack propagation, whereby the 45° angle had superior even stress distribution than the 90° angle [36–38].

3.3. ANOVA Analysis for Optimization

From the ANOVA table, it is clear that all five mechanical response models are statistically fit and reliable for the prediction of FDM-printed components' behavior. The statistical significance of all five models is demonstrated by p-values ranging between 0.0016 and 0.045 (all of which are less than 0.05), proving that there is an actual impact made by factors taken into account on particular responses. Secondly, R^2 values vary from 0.652 to 0.878, so that models account for 65% to 88% of the variance in analyzed responses. Most importantly, however, all five models display positive values of predicted R^2 (varying from 0.482 to 0.625) close to adjusted R^2 values, thus proving that overfitting is absent and the models are able to predict new values accurately. Adequate precision values vary from 6.12 to 9.80. Table 7: Anova Analysis for Tensile Stress

The model of Young's modulus is linear, whereas all others need to have a quadratic model since they exhibit non-linearity. While the model for Tensile test at break has relatively high variance (19.55% CV), it is still acceptable. Conclusion: This ANOVA table guarantees that all five models will be suitable for their intended purpose.

The statistical outputs obtained from ANOVA analysis prove that all developed models are statistically significant and suitable for modeling the experimental data. The Young's Modulus and the Flexural Stress have the best modeling results because the obtained R^2 values are very high, close to 1, as well as there is a high correspondence between the adjusted and predicted R^2, and the coefficient of variations is very low at only 1.77% and 2.63%, correspondingly. For the Flexural Strain and Flexural Displacement, the obtained R^2 equals 0.8600; thus, it means that the developed models fit the data quite well. At the same time, the adjusted and predicted R^2 values are also appropriate, and it indicates that the models can be used as predictors despite the relatively high variation of data. Adequacy Precision for all responses is higher than 4; thus, the signal-to-noise ratio is satisfactory. Table 8: represent the ANOVA analysis for tensile stress

3.4. RSM Analysis for Optimization

The RSM optimization was designed to maximize stiffness properties (Young's modulus, ultimate tensile strength, UTS) and minimize ductility parameters (displacement, strain) in order to achieve structurally balanced composites with optimal load-carrying and deformation resistance. The optimization strategy used investigated the effects of the influence of the main input factors, raster angle (A), raster width (B), and fiber density (C). RSM illustrates the interaction relationships between factors by mapping the path of steepest ascent and identifying a stationary point on a three-dimensional response surface. 3D contour plots provide a more detailed view of parameter interactions compared to 2D plots, illustrating the nonlinear relations and synergistic effects of raster angle, width, and fiber density on mechanical behavior. The responses of the values examined by RSM for the tensile test: predicted vs. actual plot, and 3D plot against raster angle and width are presented in Fig. 12 to Fig. 16.

The predicted vs. actual plot for Young's modulus is shown in Fig. 12, which confirms the predictive power of the model, characterized by high linearity between the calculated and measured Young's modulus, a small residual error, and a high quality of the RSM regression fit. A raster angle of 45° and raster width of 0.5 mm optimizes Young's modulus by facilitating effective diagonal load transfer, enhancing interlayer adhesion, and minimizing void formation during deposition. This trend quantitatively establishes the same conclusion that such parameters favour maximum stress transfer and adhesion of layers, with the model reaffirming that deviations, particularly to increased widths or 90° angles, lead to a progressive reduction in stiffness due to decreased interfacial bonding as well as greater void content.

The predicted and actual values of ultimate tensile stress are closely matched, with the RSM model confirming this to establish robustness. Fig. 13 indicates high sensitivity of UTS to raster angle and width, validating that a 45° raster angle and 0.5 mm width provide the best interfacial cohesion and load alignment. It highlights that these parameters are critical for achieving maximum UTS. The model numerically demonstrates that greater raster widths or deviations from 45° decrease UTS, which is probably caused by lower interlayer cohesion and unoptimized load transfer, with the surface plot easily showing the reduction as parameters deviate from the optimum. The colour transition from cool (blue to green) to warm signifies a localized optimum to ensure narrower raster widths and fibre diagonal orientation,

Table 8
ANOVA Analysis for Flexural Analysis.

Insignificant factors	Young's Modulus	Flexural Stress	Flexural Strain	Flexural Displacement
Standard Deviation (SD)	65.57	1.57	0.0446	0.0571
Mean	3706.34	59.99	1.78	2.31
CV %	1.77	2.63	2.50	2.47
R^2	0.9893	0.9885	0.8600	0.8600
Adjusted R^2	0.9797	0.9782	0.7900	0.7850
Predicted R^2	0.8420	0.8110	0.7300	0.7200
Adeq Precision	31.68	27.41	9.20	9.10
F-Value	32.79	35.21	8.50	8.20
P-Value	0.0001	0.0002	0.0015	0.0018
Lack of Fit	0.0004	0.0002	0.0010	0.0012
% of Noise	0.07	0.03	0.07	0.06

Table 7
Anova Analysis for Tensile Stress.

Insignificant factors	Young's Modulus	Ultimate Tensile Stress	Tensile Test at Break	Displacement at Break	Tensile Strain
Model	Linear	Quadratic	Quadratic	Quadratic	Quadratic
Standard Deviation	438.36	3.75	4.46	0.2216	0.1438
Mean	4013.18	36.02	22.83	2.53	1.46
CV (%)	10.92	10.40	19.55	8.75	9.85
R^2	0.6520	0.8782	0.7015	0.8358	0.8610
Adjusted R^2	0.5810	0.7685	0.6020	0.7205	0.7520
Predicted R^2	0.5230	0.6250	0.4820	0.5520	0.5710
Adeq Precision	6.85	8.1154	6.12	8.9109	9.8010
F-Value	5.12	8.01	3.85	5.65	6.88
P-Value	0.0125	0.0016	0.0450	0.0061	0.0029
% of Noise	0.11	0.10	0.20	0.09	0.10

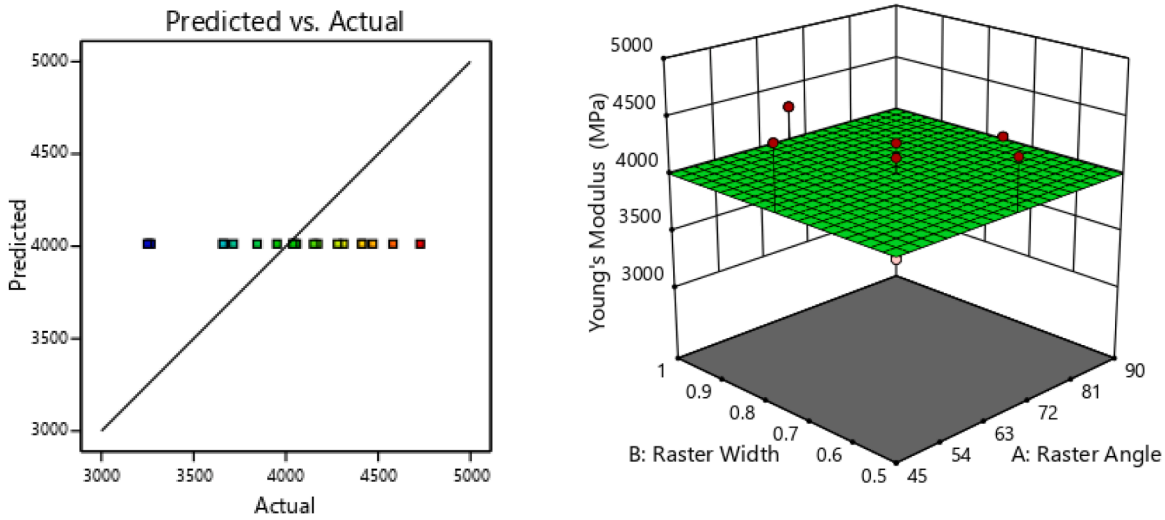

Fig. 12. Response for Young's modulus: (a) Predicted vs. Actual plot, and (b) 3D response surface plot against raster angle and width.

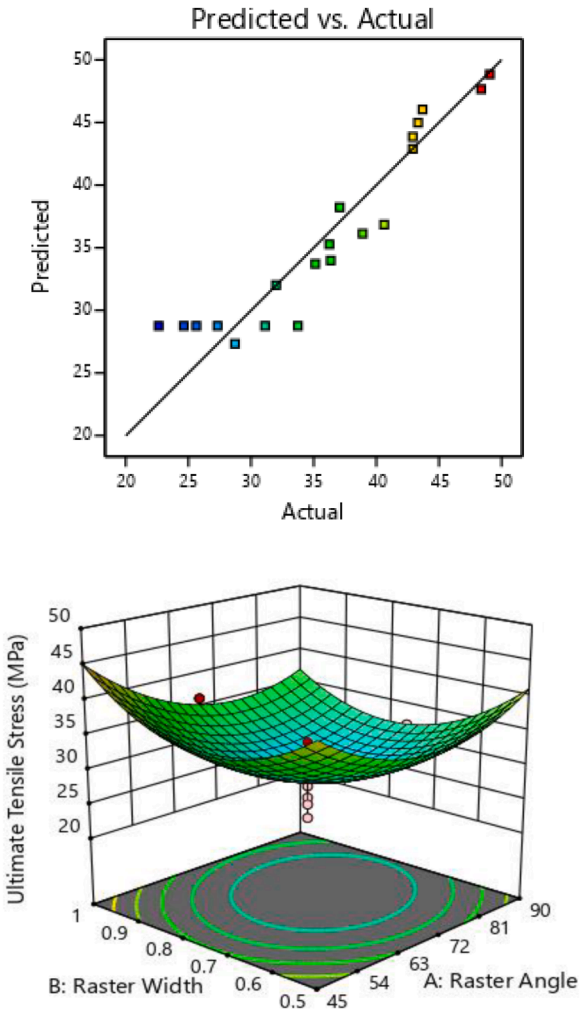

Fig. 13. Response for Ultimate Tensile Stress: (a) Predicted vs. Actual plot, and (b) 3D response surface plot against raster angle and width.

maximizing tensile load-carrying capacity.

Fig. 14 shows that the predicted and actual plot sizes for tensile stress at break are in good agreement, indicating the reliability of the model. The 3D response surface plot versus raster angle and width indicates that stress at break is maximum at 45° and 0.5 mm, with the surface having a similar but wider peak than the UTS. A wider peak means the performance is less sensitive to small changes in the parameters. This indicates that although the identical parameters optimize this response, it can be slightly less responsive to fluctuations. However, the model still predicts a decrease at wider widths and 90° angles due to intensified defect creation and substandard fiber matrix consistency.

The actual and predicted values for displacement at break are in good agreement, verifying the appropriateness of the model for ductility-related responses. Fig. 15 indicates that the 3D surface map shows that the displacement is maximal under a 45° raster angle and at reasonable raster widths (from 0.5 to 0.75 mm), and that the surface has a gentle slope without sharp peaks. The 45° angle enhances stress transmission and layer adhesion, enabling more efficient energy absorption and delaying fracture. Because ductility depends more on this inter-layer bonding mechanism than on the width of individual strands, raster width has a less severe influence.

The RSM-calculated versus experimental results are consistent with experimental strain values, ranging from 1.1 to 2.2% (Fig. 16). The surface at 3D possesses a broad valley where tensile strain decreases at a 45° raster angle and a width of 0.5 mm, particularly at 10 to 20 wt.% flax. The tensile strain at 45° and 0.5 mm is reduced due to limited chain mobility and a high degree of interlayer adhesion, making the material more resistant to deformation. However, higher flax content further restricts polymer chain mobility, reducing ductility. Decreased ductility is indicated by blue to green colour valleys, and strain increases moderately at 45° and a width of 1 mm. The flattened profile near the trough indicates favorable conditions for achieving low strain with reduced sensitivity to small parameter changes.

The DOE optimization identified an optimal parameter region at approximately 9.6 wt.% flax fiber, 0.57 mm raster width, and 44° raster angle, with a desirability of 0.87 (87%) . A maximum Young's modulus of 4465.64 MPa and a fracture tensile strength of 38.32 MPa correspond to the optimal values of 10 wt% flax fiber, a raster width of 0.5 mm, and a raster angle of 45°. It confirms significant improvements in stiffness, load transfer efficiency, and interlayer bonding, indicating an improvement in stiffness, load transfer performance, and inter-layer binding properties of composite layers. Improved stiffness and load transfer performance can be achieved due to better stress transfer from the matrix to the fibers in moderate fiber volume content (FVC), at which point fiber reinforcements effectively resist deformation without agglomeration. Likewise, the raster angle of around 45° ensures relatively uniform stress distribution along deposition trajectories while providing good layer-to-layer adhesion, while decreased raster width

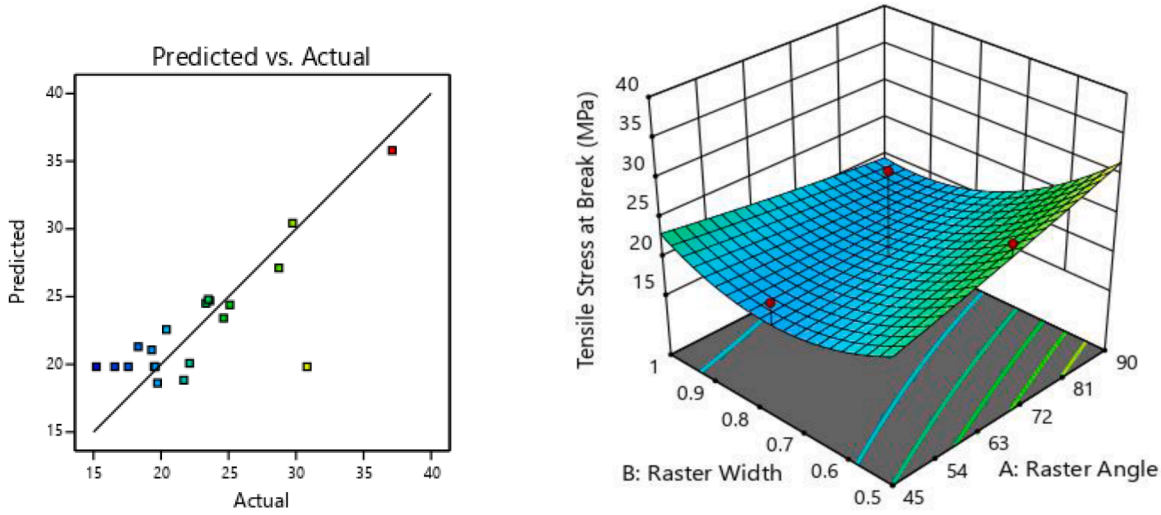

Fig. 14. Response for Tensile Stress at Break: (a) Predicted vs. Actual plot, and (b) 3D response surface plot against raster angle and width.

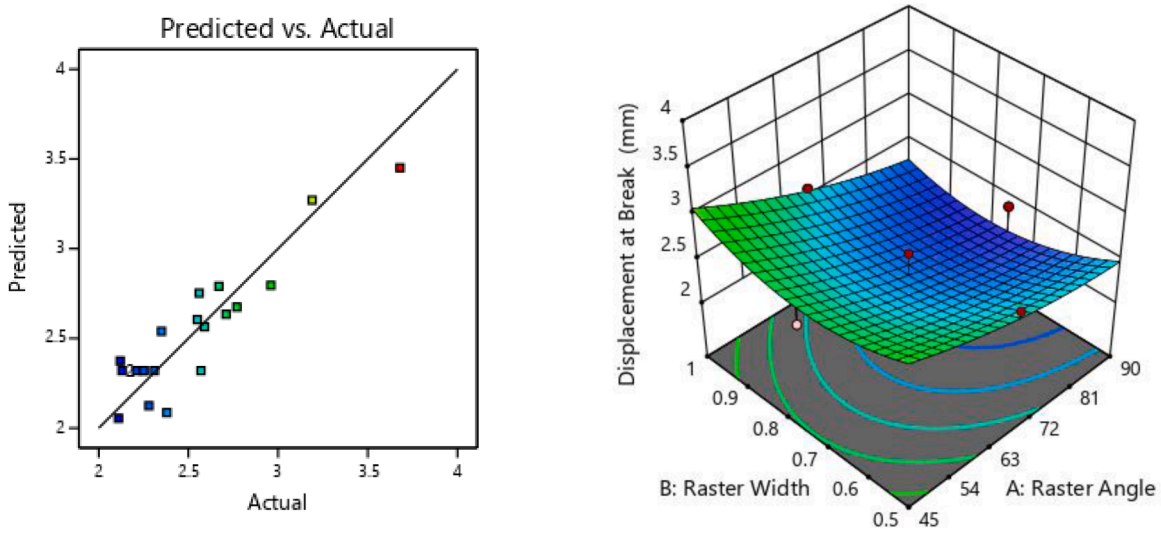

Fig. 15. Response for Displacement at break: (a) Predicted vs. Actual plot, and (b) 3D response surface plot against raster angle and width.

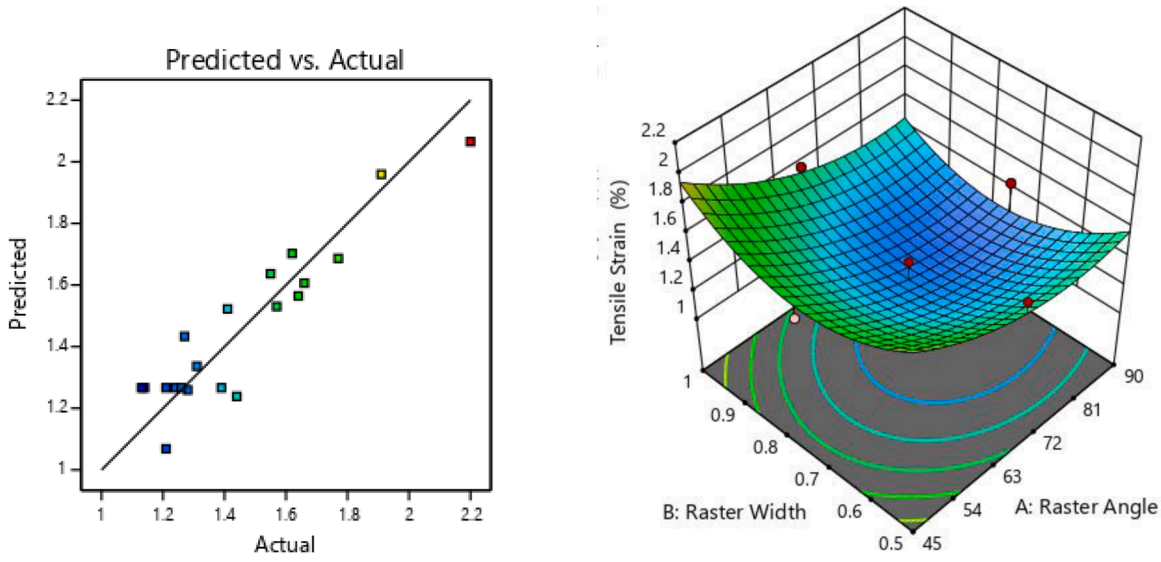

Fig. 16. Response for Tensile Strain: (a) Predicted vs. Actual plot, and (b) 3D response surface plot against raster angle and width.

provides better filament overlap and minimizes porosity, allowing improved bead fusion. The obtained high desirability value and close agreement between the model's predictions and experimentally obtained values confirm good prediction capability of the model used. Small deviations of actual values from predicted values are considered acceptable. Furthermore, the maximum values obtained from a single characteristic indicate its optimal performance, the optimal combination gives the best tradeoff for performing multiple responses, making it more appropriate for structural applications where multiple mechanical performances are needed [26,27].

RSM optimization identified raster angle, raster width, and fiber density as influencing the tensile properties of the composites produced and confirmed that raster angle was the most influential parameter. Fig. 16 indicates that a 45° raster angle and 10 wt.% flax are the optimal configurations for flexural strength, as this provides symmetrical fiber alignment and matrix bonding for effective stress transfer. Maximum Young's Modulus (4728.12 MPa) was achieved at 45° raster angle, 1 mm raster width, and 20 wt.% fiber and clearly shows that reinforcement with fiber increases stiffness; nevertheless, very high fiber loading periodically decreased modulus, consistent with evidence that poor fiber–matrix dispersion can lead to stress concentrations. Tensile Stress at Break was optimized (37.12 MPa) at a 90° raster angle and 0.5 mm width with no fibers, although fiber addition usually reduces performance, consistent with previous work, which ascribes decreased break stress to fiber-matrix debonding. The above findings support the notion that a 45° raster angle provides the most desirable orientation for load transfer, as previously demonstrated in research. The findings validate a stiffness-ductility trade-off that is optimal at a 45° raster angle, 1 mm raster width, and low-to-moderate fiber density (0–10 wt.%). However, high fiber addition (20 wt.%) should be avoided in tensile use, as it negatively impacts UTS and strain. The responses of the values examined by RSM for the flexural test: predicted vs. actual plot, and 3D plot against raster angle and width are presented in Fig. 17 to Fig. 20.

Fig. 17 presents a very strong positive relationship with the data points clustered closely along the line of best agreement, as shown in the predicted vs. actual plot for flexural stress. The 3D response surface plot, most probably plotted with two important factors, raster angle and infill density, while keeping raster width at its optimal value (0.5 mm), would have a clear curved peak. The peak determines quantitatively the set of 45° raster angle and 10 wt.% flax infill as the global maximum for the flexural strength, with the forecasted optimum value of 73.395 MPa.

Fig. 18 graphically illustrates the strong correlation between raster angle and the width of the corresponding 3D surface plot. Furthermore, by keeping the fill density constant at 10% and varying the raster angle and width, the predicted vs. actual map further confirms the reliability of the model. A 45° raster angle combined with a small raster width of 0.5 mm. The map demonstrates a steep decline in stress levels with increasing raster width beyond this value, which would indicate that the flexural stress is optimal in a certain area of the surface. The map graphically illustrates how higher widths create less solid interlayer bonds and higher void content, both of which are detrimental to flexural performance. The 45° slope continues as the surface crest, highlighting its dominance. Flexural stress decreases at widths beyond 0.5 mm due to increased bead size, creating voids and poor interlayer fusion, compromising structural integrity even with the ideal 45° raster angle.

The optimal displacement under almost the same conditions at 45° and medium-sized raster widths (e.g., 0.6–0.7 mm) is seen in Fig. 19, which forms a plateau region on the surface that reflects that the flexural displacement is stabilized by uniform layer adhesion and controlled plastic deformation before fracture. The 45° angle is most optimal for providing layer integrity and plastic deformation, while the narrow width (0.5 mm) is most controllable. The flexural displacement is stabilized by uniform layer adhesion and controlled plastic deformation before fracture. The surface mainly reflects the adverse effect of high fiber content (≥20 wt.%) on ductility, as the surface decreases as a result of enhanced brittleness due to fiber aggregation.

The actual vs. predicted plot for Young's modulus represents an excellent fit, confirming the model's ability to reproduce the parameters controlling stiffness (Fig. 20). The 3D response surface plot for this property is particularly dramatic, often indicating a well-defined and sharp peak. The plot shows a steep slope, meaning small changes in angle or width cause large changes in modulus. This visual steepness directly indicates high sensitivity. This peak occurs directly at the intersection of the 45° raster angle and the 0.5 mm raster width, which visually supports the conclusion that this composition is important for increasing stiffness (4453.85 MPa). The vertical slopes on each side of this peak qualitatively demonstrate the large sensitivity of stiffness to these parameters. The surface shows a spectacular drop at an angle of 90°, where the load is weakly transferred between the layers, and a comparable drop with increasing raster widths, where the high porosity and low bond area weaken the structural integrity and effective load-bearing cross-section.

Results showed that the optimum value was achieved at the optimal parameter set of 10 wt.% flax filler, a raster width of 0.5 mm, and a raster angle of 45 °. It provides high interlayer bonding density and stress distribution, and excellent stiffness-to-strength ratio with low brittleness. This was predicted to result in an optimal balance of stiffness and strength, with a maximum Young's modulus of 4453.85 MPa and a maximum flexural stress of 73.395 MPa. The main strength of RSM is its ability to fit a multidimensional response surface to the experimental

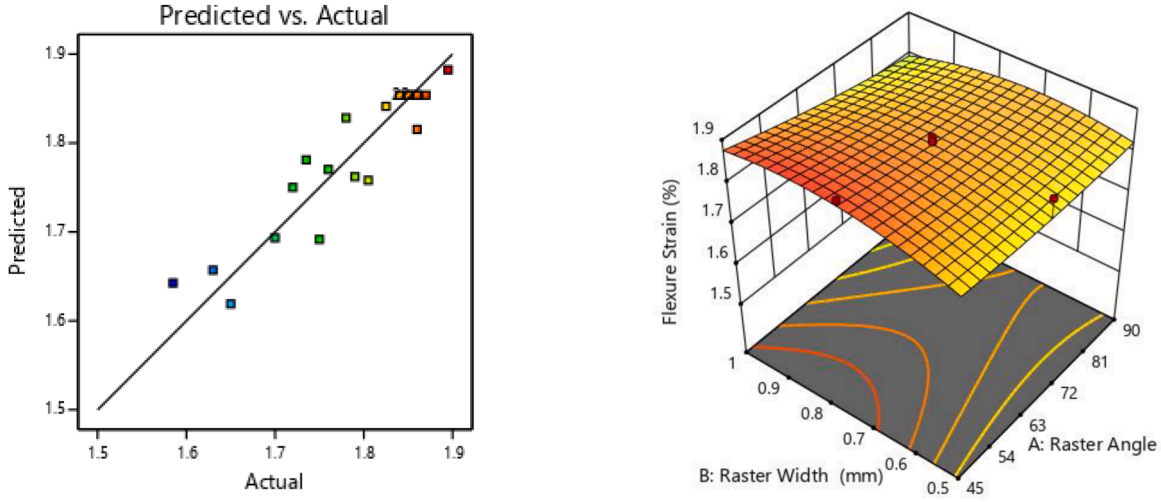

Fig. 17. Response for Flexure Strain: (a) Predicted vs. Actual plot, and (b) 3D response surface plot.

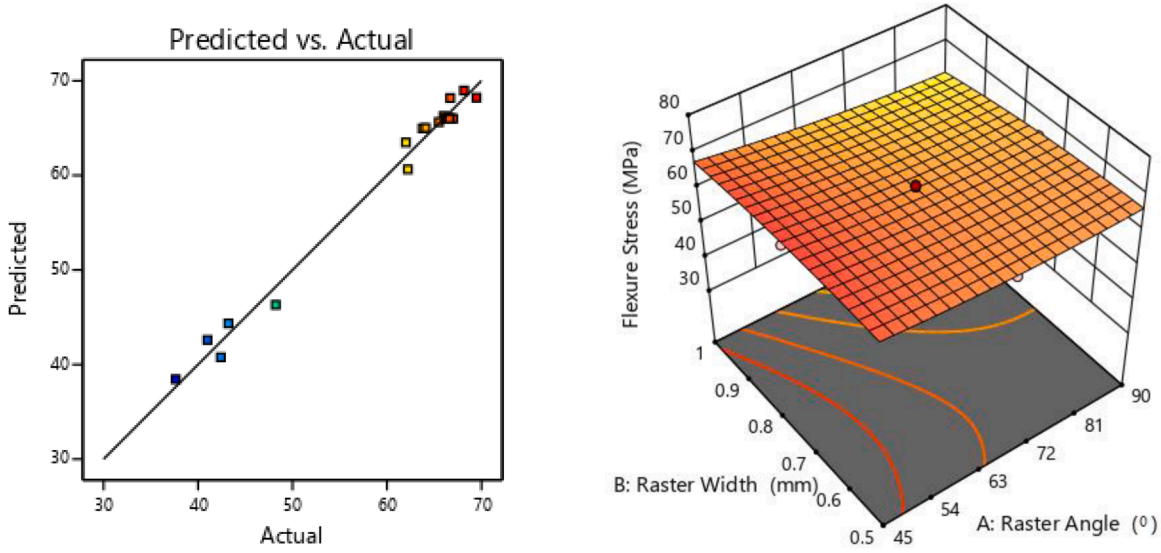

Fig. 18. Response for Flexture Stress: (a) Predicted vs. Actual plot, and (b) 3D response surface plot.

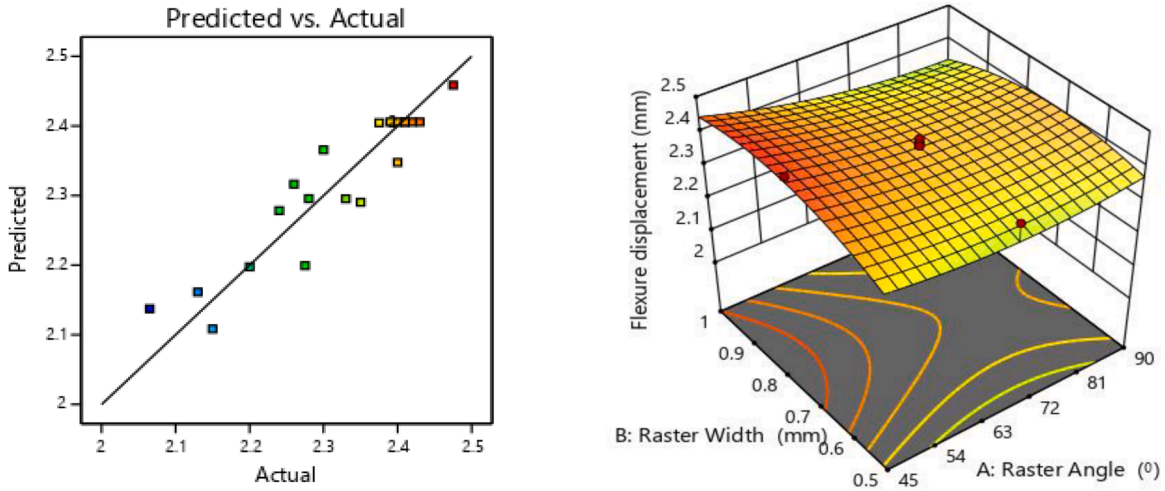

Fig. 19. Response for Flexure Displacement: (a) Predicted vs. Actual plot, and (b) 3D response surface plot.

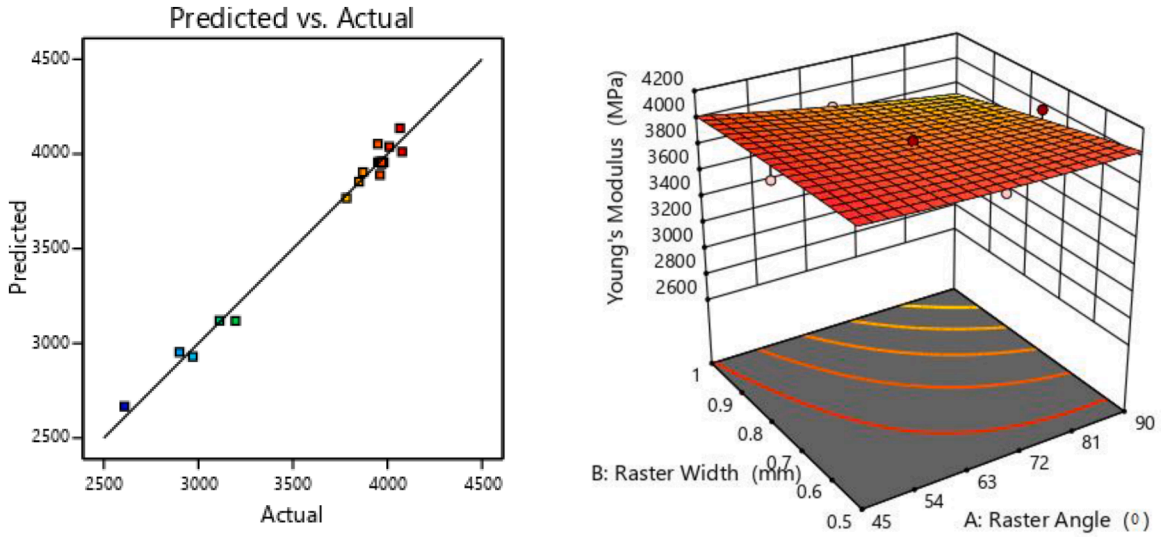

Fig. 20. Response for Young's modulus: (a) Predicted vs. Actual plot, and (b) 3D response surface plot.

data, revealing that fiber density has a quadratic effect, where performance decreases above 10 wt.% due to consolidation and increased viscosity, the 45° raster angle dominates due to superior load transfer and stress distribution, and the narrow 0.5 mm raster width promoted dense deposition and strong interlayer bonding. Up to 10%, fibers reinforce the matrix, but beyond that, they agglomerate and create stress concentration points. This thereby provides a rigorous, model-based interpretation that directly links process parameters to the final mechanical properties. Table 9 represent the comparative analysis of existing study.

Finally, this study demonstrates the effectiveness of a response surface methodology (RSM) system in modeling and optimizing the FDM 3D printing parameters of Harakek fiber-reinforced PLA composites. The investigation confirmed that the best parameters, in particular 10 wt.% fiber content, 45° raster angle, and 0.5 mm raster width, resulted in the best synergy of tensile and flexural properties, as indicated by a Young's modulus of 4453.85 MPa and a flexural stress of 73.395 MPa. The desirable function value was 0.91, and the excellent correlation between the predicted and measured results further confirms the validity of the RSM model, closely aligning with the experimental values. The presented RSM overlay diagram clearly provides this workable design space. The determined parameters help to achieve improved mechanical performance for lightweight structures, thereby providing a strong foundation for future material innovations. The shortcomings of the experiment include the fact that only tensile strength and flexural strength have been tested. In order to confirm the feasibility of using these materials in construction, further research needs to be done to test other characteristics, including impact strength, fatigue strength, environmental resistance, anisotropy of FDM products, and microstructure.

Table 9
Comparative Analysis with Existing Study.

Study	Material System	Tensile Strength (MPa)	Young's Modulus (MPa)	Flexural Strength (MPa)	Ref
Present work	PLA + Flax fiber (9.6–10 wt.%)	38.32	4453.85	73.40	_
Nanovia (2023)	PLA + Flax fiber	41.00	3100.00	—	[39]
Uddin (2024)	PLA + Hemp fiber (5 wt.%)	35.00	—	86.00	[40]
Akonda et al. (2018)	PLA + Flax (compression molded)	151.00	18500.00	215.00	[41]
Bamboo fiber study (2026)	PLA + Bamboo fiber (9 wt.%)	80.68	—	128.48	[42]
Date palm fiber study (2025)	PLA + Date palm fiber (5 wt.%)	53.69	—	—	[43]
PLA/Glass fiber (2025)	PLA + Glass fiber	59.27	—	85	[44]

4. Conclusions

In conclusion, this study successfully developed and analyzed the RSM-based optimization model to improve the tensile and flexural properties of harakeke (New Zealand flax) fiber–reinforced PLA composites printed using FDM 3D printing. It is found that the optimal values of 10 wt.% flax fiber, 0.5 mm raster width, and 45° raster angle greatly improved the stiffness, load transfer efficiency, and interlayer bonding, with a maximum Young's modulus of 4453.85 MPa and flexural stress of 73.395 MPa. Furthermore, the findings clearly indicate that raster angle has the most significant effect on stress distribution, with reduced raster widths increasing print density and enhancing bonding integrity. But increasing fiber content above 10 wt.% resulted in fiber agglomeration and decreased strength, mirroring the processing constraint of high-viscosity bio-composites. Despite these gains, challenges remain in achieving improved fiber dispersion at higher loadings and suppressing the voids characteristic of the FDM process. Future work should focus on more sophisticated surface treatments of flax fibers, nanoscale filler hybrid reinforcement, and multi-objective optimization that combines thermal and durability analyses. Furthermore, inclusion of data-driven machine learning models can further improve parameter prediction and process robustness. Overall, the results confirm that accurate optimization of printing parameters is crucial for unlocking the structural potential of flax–PLA composites for scalable, lightweight, and sustainable engineering applications.

Conflict of interests

The authors declare that they have no known competing financial interests or personal relationships that could have appeared to influence the work reported in this paper.

CRediT authorship contribution statement

S.K. Selvamani: Writing – original draft, Methodology, Investigation, Formal analysis, Data curation. **K.S. Clint:** Writing – original draft, Methodology, Investigation, Formal analysis, Data curation. **M. Samykano:** Writing – review & editing, Supervision, Resources, Project administration, Conceptualization. **K. Kadirgama:** Writing – review & editing, Validation, Software, Methodology. **M.D.H. Beg:** Writing – review & editing, Visualization, Validation, Resources, Conceptualization. **K.L. Pickering:** Writing – review & editing, Visualization, Validation, Resources, Conceptualization. **A. Megalingam:** Writing – original draft, Formal analysis, Data curation, Conceptualization.

Declaration of competing interest

The authors declare that they have no known competing financial interests or personal relationships that could have appeared to influence the work reported in this paper.

Acknowledgements

The authors gratefully acknowledge Universiti Malaysia Pahang, Al-Sultan Abdullah, Malaysia, for providing funds and facilities under research grant RDU192216 to conduct this research, and the United Arab Emirates University for the facilities provided.

Data availability

Data will be made available on request.

References

[1] V. DeStefano, S. Khan, A. Tabada, Applications of PLA in modern medicine, Eng. Regen. 1 (2020) 76–87.
[2] N-A Taib, M. Rahman, D. Huda, K. Kuok, S. Hamdan, M.K. Bakri, et al., A review on poly lactic acid (PLA) as A biodegradable polymer, Polym. Bull. 1 (2022) 1–35.
[3] N.G. Khouri, J.O. Bahú, C. Blanco-Llamero, P. Severino, V.O.C. Concha, EB. Souto, Polylactic acid (PLA): Properties, synthesis, and biomedical applications – A review of the literature, J. Mol. Struct. 1309 (2024) 138243.
[4] C. Zengwen, H. Pan, Y. chen, J. Bian, L. Han, H. Zhang, et al., Transform poly (lactic acid) packaging film from brittleness to toughness using traditional industrial equipments, Polymer 180 (2019) 121728.
[5] H-A Aisyah, E. Hishamuddin, A-W Noorshamsiana, Z. Ibrahim, R-A Ilyas, Oil palm fiber hybrid composites: a recent review, J. Renew. Mater. 12 (10) (2024) 1661–1689.
[6] C.S. Kannan, R. Ramesh, R. Raviram, M. Aadithya, Study of mechanical properties of sustainable biocomposite panels using Jute-PLA and Sisal-PLA, in: Materials Today: Proceedings, 2023.
[7] M. Mohammed, M.S.M. Rasidi, A. Muhana, A.R. Rozyanty, A.F. Osman, T. Adam, et al., Interfacial bonding mechanisms of natural fibre-matrix composites: An overview, BioResources 17 (2022).

[8] S. Chahdoura, R. Bahloul, M. Tlija, A. Tahan, Multi-objective optimization of PLA-FDM parameters for enhancement of industrial product mechanical performance based on GRA-RSM and BBD, Prog. Addit. Manuf. 10 (2) (2025) 1355–1383.
[9] A. Megalingam, R. Rajamony, M. Perumal, S. Malliga, Deformation behaviour of 3D printed reinforced hydroxyapatite/gelatin bio-ceramics, Int. J. Adv. Sci. Eng. 10 (2023) 3471–3481.
[10] M. Laurenti, I. Bavasso, E. Palazzi, J. Tirillò, F. Sarasini, F. Berto, Predicting the mechanical behavior in FDM printing of biopolymers through boosting artificial neural networks, Mater. Des. 257 (2025) 114475.
[11] N. Ridzuan, Z. Yaacob, F. Adam, Response surface methodology on wax deposit optimization, Malays. J. Anal. Sci. 21 (2017) 452–459.
[12] S.M. Asaad, A. Inayat, C. Ghenai, A. Shanableh, Response surface methodology in biodiesel production and engine performance assessment, Int. J. Thermofluids 21 (2024) 100551.
[13] S.M. Yahya, M. Danish, A. Ahmed, A. Equbal, Z.A. Khan, M. Asjad, RSM based optimization of process parameters of biodiesel production from waste palm oil using modified nano-catalyst, npj Clean Energy 1 (1) (2025) 1.
[14] RJGR Nimal, R. Sabarish, J.M. Jones, D.F.M. Jose, R. Sangamaeswaran, Mechanical and metallurgical characterization of polylactic acid and natural fiber composite manufactured by fused deposition modeling, Lect. Notes Mech. Eng.; (2026).
[15] W. Xu, M. Li, Y. Xu, A. Entezari, J. Fang, Mechanical Characterization of fused deposition modeling-printed wood-polylactic acid composites under water conditioning, Polym. Compos. 47 (6) (2026) 5205–5221.
[16] A. Kolhe, S. Karale, P. Anerao, Y. Munde, Mechanical characterization of 3D-printed banana fibers reinforced PLA biocomposite, SSRG Int. J. Mech. Eng. 11 (10) (2024) 74–84.
[17] M. Khasheiee-Varnamkhasti, A. Ansaripour, M. Heidari-Rarani, M. Mirsayar, Fracture behavior of natural fiber-reinforced PLA/TPU hybrid composites produced by material extrusion additive manufacturing, Fatigue Fract. Eng. Mater. Struct. (2026).
[18] A.F.J. Al-Kaabi, J.Y. Abdullah, Y. Johari, A.M. Abdullah, M.F. Yhaya, N. Hasbullah, Comparative evaluation of two bleaching solutions on Kenaf fiber-reinforced nylon: Surface properties and FTIR analysis, Adv. Mater. Res. 14 (5) (2025) 417–427.
[19] A.H. Jamadi, N. Razali, S.D. Malingam, MM. Taha, Effect of Fibre size on mechanical properties and surface roughness of PLA composites by using fused deposition modelling (FDM), J. Renew. Mater. 11 (8) (2023) 3261–3276.
[20] A. Kolhe, S. Karale, P. Anerao, Y. Munde, Mechanical characterization of banana fibers/PLA biocomposite samples produced by fused deposition modeling based 3D Printing Using Taguchi Method, SSRG Int. J. Mech. Eng. 11 (8) (2024) 84–94.
[21] M. Müller, P. Jirků, V. Šleger, R.K. Mishra, M. Hromasová, J. Novotný, Effect of infill density in FDM 3D printing on low-cycle stress of bamboo-filled PLA-based material, Polymers 14 (22) (2022).
[22] A. Wang, X. Tang, Y. Zeng, L. Zou, F. Bai, C. Chen, Carbon fiber-reinforced PLA composite for fused deposition modeling 3D printing, Polymers 16 (15) (2024).
[23] Q. Ding, X. Li, D. Zhang, G. Zhao, Z. Sun, Anisotropy of poly(lactic acid)/carbon fiber composites prepared by fused deposition modeling, J. Appl. Polym. Sci. 137 (23) (2020).
[24] X. Zhao, L. Liang, F. Mo, S. Dong, C. Deng, S. Liao, et al., Environment friendly, renewable and sustainable natural fiber-reinforced polylactic acid (PLA) composites, Polym. Compos. (2026).
[25] PLA Damage Properties in FDM Printing: A Hybrid Experimental and Machine Learning Study, in: M. Dhouioui, B. Ben Fraj, H. Hentati, M. Ben Amar, M. Haddar (Eds.), Lecture Notes in Mechanical Engineering, 2025.
[26] I. Khan, A. Al Rashid, M. Koç, Machine learning, response surface method, microscopic analysis, and optimization for mechanical properties of electrically conductive polymer composite fabricated via additive manufacturing, Oxf. Open Mater. Sci. 6 (1) (2026) itag004.
[27] I. Khan, A. Al Rashid, M. Koç, Machine learning prediction of raster angle effects on mechanical properties of extrusion-based additively manufactured conductive thermoplastic polyurethane composites, Macromol. Mater. Eng. 311 (2) (2026) e00248.
[28] J.O. Akindoyo, K. Pickering, M.D. Beg, M. Mucalo, Combined digestion and bleaching of New Zealand flax /harakeke fibre and its effects on the mechanical, thermal, and dynamic mechanical properties of poly(lactic) acid matrix composites, Compos. A: Appl. Sci. Manuf. 164 (2023) 107326.
[29] M. Tahir, A-F. Seyam, Greening fused deposition modeling: a critical review of plant fiber-reinforced PLA-based 3D-printed biocomposites, Fibers 13 (5) (2025) 64.
[30] K. Elhattab, S.B. Bhaduri, P. Sikder, Influence of Fused Deposition Modelling Nozzle Temperature on the Rheology and Mechanical Properties of 3D Printed β-Tricalcium Phosphate (TCP)/Polylactic Acid (PLA) Composite, Polym 14 (6) (2022).
[31] N. Saba, M. Jawaid, MTH. Sultan, 1 - An overview of mechanical and physical testing of composite materials, in: M. Jawaid, M. Thariq, N. Saba (Eds.), Mechanical and Physical Testing of Biocomposites, Fibre-Reinforced Composites and Hybrid Composites, Woodhead Publishing, 2019, pp. 1–12.
[32] M.N. Bashir, J.S. Lee, M.A. Bou-Rabee, H.G. Mohamed, D. Zhou, I.A. Badruddin, et al., Investigation of process parameter influence on the mechanical properties of FDM-printed PEEK-carbon fiber composites using RSM and Taguchi methods, J. Mater. Res. Technol. 36 (2025) 10199–10209.
[33] S.K. Selvamani, K. Rajan, M. Samykano, R.R. Kumar, K. Kadirgama, RV. Mohan, Investigation of tensile properties of PLA–brass composite using FDM, Prog. Addit. Manuf. 7 (5) (2022) 839–851.
[34] A.D. Nugraha, M.L. Hakim, A. Pramana, F. Triawan, M. Handayani, Y. D. Rahmayanti, MA. Muflikhun, Fracture toughness in SPCC/CFRP hybrid laminates: Mode I and mode II perspectives, Results Eng. 24 (2024) 103090.
[35] A. Nasution, M.L. Hakim, H. Herianto, AP. Rifai, Flexural performance and interfacial bonding of PLA/ABS/HIPS composites in multi-nozzle 3D printing, J. Braz. Soc. Mech. Sci. Eng. 48 (1) (2025) 47.
[36] S. Ali, I. Deiab, S. Pervaiz, State-of-the-art review on fused deposition modeling (FDM) for 3D printing of polymer blends and composites: innovations, challenges, and applications, Int. J. Adv. Manuf. Technol. 135 (11) (2024) 5085–5113.
[37] S. Ali, I. Deiab, S. Pervaiz, A. Eltaggaz, Development of sustainable polymer composite with agro-industrial residue for biomedical applications, Polym. Eng. Sci. 65 (4) (2025) 1922–1933.
[38] S. Ali, I. Nouzil, V. Mehra, A. Eltaggaz, I. Deiab, S. Pervaiz, Integrated optimization scheme for 3D printing of PLA-APHA biodegradable blends, Prog. Addit. Manuf. 10 (1) (2025) 875–886.
[39] Nanovia PLA Flax [Internet], cited 11-04-2026]. Available from: https://nanovia.tech/en/ref/nanovia-pla-flax/, 2023.
[40] MN. Uddin, Fabrication of PLA-hemp 3D printing filaments, 2024.
[41] M. Akonda, S. Alimuzzaman, D.U. Shah, ANMM. Rahman, Physico-mechanical, thermal and biodegradation performance of random flax/polylactic acid and unidirectional flax/polylactic acid biocomposites, Fibers 6 (4) (2018) 98.
[42] S.K. Adapa, Gangi Jagadish n, S. Setti, Development of bio-reinforced PLA filaments using short bamboo fibers for enhanced mechanical performance in FDM 3D printing, J. Thermoplast. Compos. Mater. 0 (0) (2026) 08927057261439635.
[43] S.H. Mian, A. Bin Jumah, M. Saleh, J.A. Mohammed, Fabrication of PLA-date fiber biocomposite via extrusion filament maker for 3D printing and its characterization for eco-friendly and sustainable applications, Polymers 17 (19) (2025).
[44] PLA 3D Printer Filament [Internet], Available from: https://www.farnell.com/datasheets/4385364.pdf, 2024.